Department of Radio Science and Engineering

On Passive Wireless Sensors Based on Intermodulation Communication

Song Jinsong

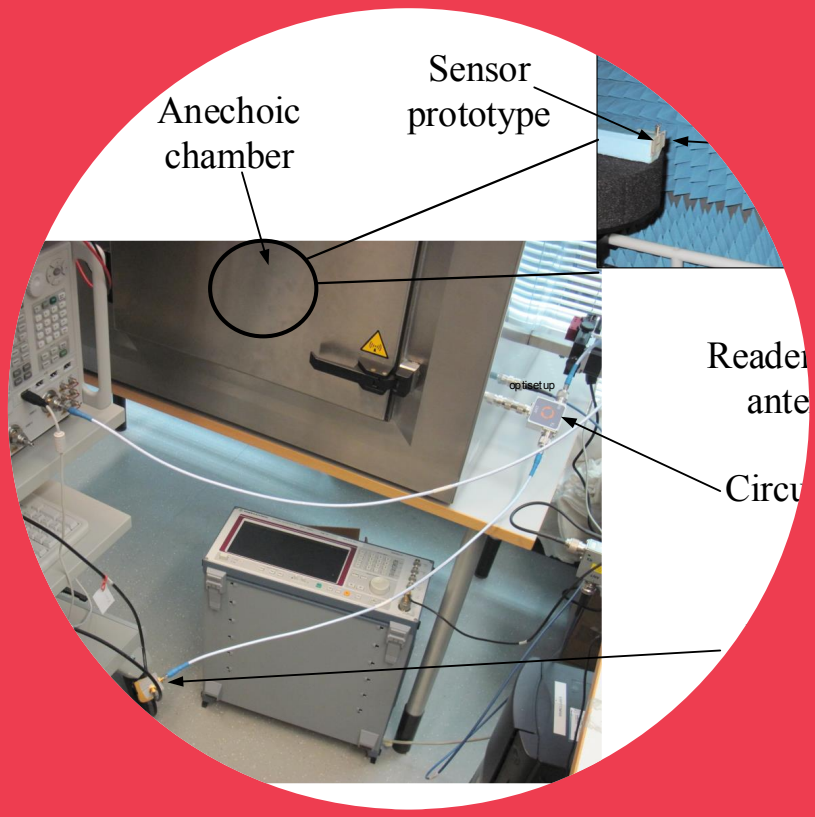

Aalto University

DOCTORAL DISSERTATIONS

Aalto University publication series
DOCTORAL DISSERTATIONS 122/2015

On Passive Wireless Sensors Based on Intermodulation Communication

Song Jinsong

A doctoral dissertation completed for the degree of Doctor of Science (Technology) to be defended, with the permission of the Aalto University School of Electrical Engineering, at a public examination held at the lecture hall S3 of the school on 9 October 2015 at 12.

Aalto University
School of Electrical Engineering
Department of Radio Science and Engineering

Supervising professor
Prof. Ville Viikari

Thesis advisor
Dr. Nadine Pesonen

Preliminary examiners
Prof. Leena Ukkonen, Tampare University of Technology, Finland
Prof. Apostolos Georgiadis, Centre Tecnologic de Telecomunicacions de Catalunya (CTTC), Barcelona, Spain

Opponent
Prof. Smail Tedjini, Grenoble-INP, France

Aalto University publication series
DOCTORAL DISSERTATIONS 122/2015

ISBN 978-952-60-6354-6 (printed)
ISBN 978-952-60-6355-3 (pdf)
ISSN-L 1799-4934
ISSN 1799-4934 (printed)
ISSN 1799-4942 (pdf)
http://urn.fi/URN:ISBN:978-952-60-6355-3

Unigrafia Oy
Helsinki 2015

Finland

441 697
Printed matter

Author
Author

Name of the doctoral dissertation
On Passive Wireless Sensors Based on the Intermodulation Communication

Publisher School of Electrical Engineering

Unit Department of Radio Science and Engineering

Series Aalto University publication series DOCTORAL DISSERTATIONS 122/2015

Field of research Radio Engineering

Manuscript submitted 18 June 2015 **Date of the defence** 9 October 2015

Permission to publish granted (date) 19 August 2015 **Language** English

☐ **Monograph** ☒ **Article dissertation (summary + original articles)**

Abstract

Wireless sensors are needed in applications where a wired connection is difficult. Wireless sensors are often equipped with a radio transceiver and a battery or another energy source. These energy sources may limit life-time or operation conditions, and increase the size and cost of wireless sensors.

Wireless sensors can also be passive. Due to the limited energy available for these sensors, they typically only support relatively short communication distances and may not provide a means for identifying a certain sensor. This dissertation develops a certain type of passive wireless sensors called the intermodulation communication sensors. This type of passive wireless sensor may potentially have many advantages compared with other passive wireless sensors.

Intermodulation communication sensors have been developed in many ways in this dissertation. One challenge was that they were difficult to make compliant with frequency regulations due to the relatively large band needed. This dissertation shows how the bandwidth required can be reduced significantly by using a Quartz crystal or other mechanical resonators. It is also demonstrated that such a resonator enables the utilization of a generic capacitive sensing element in the sensor, making it possible to monitor a broad set of variables. Furthermore, it is shown how intermodulation sensors can be made identifiable.

Despite the fact that the studied sensor circuits are fairly simple, many important parameters, such as the read-out distance and measurements resolution strongly depend on the selected circuit components. This dissertation derives design equations for one specific sensor circuitry. The design equations help to choose proper component values in order to achieve the best possible read-out resolution.

Passive wireless sensors are often used in large volume applications where low sensor fabrication cost is important. Unit fabrication costs of electronic circuits can typically be lowered by increasing volumes and the integration level. This dissertation studied how the integration of intermodulation communication sensors could be increased by integrating all the passives.

The intermodulation communication sensors are interrogated with a specific reader device. This dissertation has contributed to the development and realization of a reader device whose limitations affecting reader performance are studied. The reader device also needs to estimate the sensor state from the measured intermodulation response of the sensor. Furthermore, this dissertation has contributed to the development of an estimation algorithm for the sensor state.

Keywords Mixers, Intermodulation communication, Passive wireless sensors, RFID

ISBN (printed) 978-952-60-6354-6 **ISBN (pdf)** 978-952-60-6355-3

ISSN-L 1799-4934 **ISSN (printed)** 1799-4934 **ISSN (pdf)** 1799-4942

Location of publisher Helsinki **Location of printing** Helsinki **Year** 2015

Pages 152 **urn** http://urn.fi/URN:ISBN:978-952-60-6355-3

Preface

The research leading to this dissertation has been mainly carried out in the Intelligent Sensor Systems group of VTT, Technical Research Centre of Finland, during the years 2012–2015. The work has been funded by Tekes and carried out in the EFFIMA–InterSync research project, the Doctoral School of Electrical Engineering, and the Nokia Foundation.

First and foremost, I would like to express my sincere respect to my supervisor Prof. Ville Viikari and thesis advisor Dr. Nadine Pesonen for supporting me in the pursuit of this doctoral dissertation and guiding me patiently during these years.It has been a great pleasure and an honor to work with them during the past years.

I would like to thank all of the other co-authors of my publications for their significant contributions to this dissertation. I would to thank all my present and former colleagues at the department of Radio Science and Engineering, Antti,Clemens, Dimtri, Eikka, Jan, Jan, Juha, Jussi, Katsu, Linsheng, Mazidul, Mikko, Mirjam, Sajjad, Subash, Timo, Tuula, Usman, Zhou, and many more. I would like to extend my sincere gratittude to my formor colleagues at VTT, Technical research centre. Thank you, Nadine, Colm, Pekka, Kaj, Juha-matti, Ilkka, Heikki and many more.

I am grateful to the pre-examiners, Prof. Leena Ukkonen and Prof. Apostolos Georgiadis, for their valuable reviews and comments to improve the quality of this dissertation. My gratitude also goes to Prof. Smail Tedjini for accepting to be the opponent during the public examination.

I would like to thank all my friends in Finland for all the enjoyable and colourful moments together.

I would like to thank my parents, Song Jie, and Li Hong, for all the support and understand in my life.

Finally, my deepest thanks go to my spouse, Su Yi. Thank you for your endless love, support, and encouragement, and thank you for bringing our

beloved son, Song William, into the world.

Helsinki, September 2, 2015,

Song Jinsong

Contents

List of Publications

This thesis consists of an overview and of the following publications which are referred to in the text by their Roman numerals.

I V. Viikari, J. Song, and H. Seppä, "Passive wireless sensor platform utilizing a mechanical resonator," *IEEE Sensors Journal*, Vol. 13, No. 4, pp. 1180–1186, April, 2013.

II J. Song, V. Viikari, N. Pesonen, I. Marttila, and H. Seppä, "Optimization of wireless sensors based on intermodulation communication," *IEEE Transactions on Microwave Theory and Techniques*, Vol. 61, No. 9, pp. 3446–3452, September, 2013.

III J. Song, J. Salmi, V. Viikari, and N. Pesonen, "Maximum Likelihood Estimation for Passive Wireless Intermodulation Communication Sensors," *IEEE Sensors Journal*, Vol. 15, No. 4, pp. 2280–2286, February, 2015.

IV J. Song, N. Pesonen, and V. Viikari, "Realizing Frequency Division Multiple Access with Passive Wireless Intermodulation Communication Sensors," *Microwave and Optical Technology Letters*, Vol. 57, No. 2, pp. 274–277, December, 2014.

V J. Song, N. Pesonen, V. Viikari, and H. Seppä, "On the Use of the Intermodulation Communication Towards Zero Power Sensor Nodes," *in Proceedings of the 43rd European Microwave Conference*, Nuremberg, Germany, pp. 124–127, 6–10 October, 2013.

VI J. Song, N. Pesonen and V. Viikari, "Long Range Passive Wireless MEMS-based Inclination or Acceleration Sensor Utilizing the Intermodulation Communication Principle," *in Proceedings of the International Wireless Symposium (IWS)*, Xi'an, China, pp. 1–4, 24–26 March, 2014.

VII J. Song, N. Pesonen, P. Pursula, and V. Viikari, "Integrated Passive Wireless Sensor Transponders based on the Intermodulation Communication Principle," *in Proceedings of International Microwave Symposium (IMS)*, Tampa, FL, pp. 1–4, 1–6 June, 2014.

VIII V. Viikari, J. Song, N. Pesonen, P. Pursula, H. Seppä, "Review of Passive Wireless Sensors Utilizing the Intermodulation Communication," *in Proceeds of RFID-TA 2014*, Tampere, Finland, pp. 56–61, 8–9 September, 2014.

IX P. Pursula, N. Pesonen, J. Song, I. Marttila, and V. Viikari, "Achieving Long Reading Ranges with Passive Wireless Intermodulation Sensors," *in Proceedings of RFID-TA 2014*, Tampere, Finland, pp. 131–134, 8–9 September, 2014.

Author's Contribution

Publication I: "Passive wireless sensor platform utilizing a mechanical resonator"

This was a result of collaborative work. The underlying idea was developed by Prof. Ville Viikari who supervised the work and contributed to the theoretical derivations and simulations. The author further elaborated the theory, conducted the experiments and helped in writing the paper.

Publication II: "Optimization of wireless sensors based on intermodulation communication"

This was the result of collaborative work. Prof. Viikari and the author developed the idea for the optimized circuit. The author was mainly responsible for carrying out the simulations, measurements, and analysis of results. The author contributed to the writing of the paper. Prof. Ville Viikari and Dr. Nadine Pesonen supervised and instructed the work.

Publication III: "Maximum Likelihood Estimation for Passive Wireless Intermodulation Communication Sensors"

The author carried out simulations and experiments and developed the signal model together with Prof. Ville Viikari. Dr. Jussi Salminen mainly contributed to deriving estimation algorithms. The paper was written in close collaboration with Dr. Jussi Salmi. Prof. Ville Viikari and Dr. Nadine Pesonen supervised and instructed the work.

Publication IV: "Realizing Frequency Division Multiple Access with Passive Wireless Intermodulation Communication Sensors"

This paper was mainly the work of the author. The idea of realizing frequency division multiple access was developed together with Prof. Ville Viikari. Dr. Nadine Pesonen provided assistance in writing the article.

Publication V: "On the Use of the Intermodulation Communication Towards Zero Power Sensor Nodes"

This was the result of close collaborative work with Dr. Nadine. Pesonen who helped in writing the article. The author derived the equations, carried out the measurements, and analyzed the results. Prof. Ville Viikari supervised the work.

Publication VI: "Long Range Passive Wireless MEMS-based Inclination or Acceleration Sensor Utilizing the Intermodulation Communication Principle"

This paper was mainly the work of the author. The idea of the publication was proposed by the author. The author carried out the experiments and analyzed the results. Moreover, the author was responsible for writing the publication. Dr. Nadine Pesonen and Prof. Ville Viikari supervised and instructed the work.

Publication VII: "Integrated Passive Wireless Sensor Transponders based on the Intermodulation Communication Principle"

This was the result of a collaborative work between all authors. The author was responsible for the theory, experiment, and analysis of the results. Dr. Pekka Pursula designed the layout of the integrated sensor and helped in writing the paper. Dr. Nadine Pesonen wrote the paper. Prof. Ville Viikari supervised the work.

Publication VIII: "Review of Passive Wireless Sensors Utilizing the Intermodulation Communication"

This was the result of a collaborative work. The idea of the paper was proposed by Prof. Ville Viikari who had the main responsibility of writing the publication. The author further elaborated the work by deriving a theoretical equation for the read-out distance and helped to write the paper.

Publication IX: "Achieving Long Reading Ranges with Passive Wireless Intermodulation Sensors"

This was a result of collaborative work with Dr. Pekka Pursula and Dr. Nadine Pesonen. The idea of the publication was proposed by Dr. Pekka Pursula. He was responsible for writing the paper. The reader diagram was proposed by Dr. Nadine Pesonen. The author was responsible for simulations, and contributed to developing the reader system, carrying out experiments, and helping to write the paper.

List of Abbreviations

A/D	Analog to Digital
AWR	A circuit simulator, AWR Corporation, 1960 E. Grand Avenue Suite 430
DC	Direct Current
ECG	Electrocardiography
FDMA	Frequency Division Multiple Access
FIMECC	Finnish Metals and Engineering Competence Cluster
FSPL	Free Space Path Loss
HF	High Frequency
HRV	Heart Rate Variability
IC	Integrated Circuit
ID	Identification
IDT	Inter-digital Transducer
IF	Intermediate Frequency
IoT	Internet of Things
IPD	Integrated Passive Device
LF	Low Frequency
LM	Levenberg-Marquardt
MEMS	Microelectromechanical Systems
MHz	Mega Hertz
PCB	Printed Circuit Board
PLL	Phase Lock Loop
PPM	Pulse Position Modulation
RF	Radio Frequency
RFID	Radio Frequency Identification
SAW	Surface Acoustic Wave
UHF	Ultra High Frequency
VNA	Vector Network Analyser
VCO	Voltage Controlled Oscillator

WSN	Wireless Sensor Networks

List of Symbols

β_x	Relative sensitivity towards a physical quantity x
γ	Profile parameter for depletion capacitance
Γ	Reflection coefficient
$\boldsymbol{\theta}$	Parameter set
$\hat{\boldsymbol{\theta}}_{ML}$	Cost function
λ	Wavelength
Φ	Built-in potential for diodes
ω	Angular frequency
ω_1, ω_2	Carrier angular frequency
ω_Δ	Difference angular frequency, $\omega_\Delta = \omega_1 - \omega_2$
ω_{IM}	Intermodulation angular frequency, $\omega_{IM} = 2\omega_1 - \omega_2$
ω_{RF}	angular frequency at RF
C_0	Capacitance of quartz crystal
C_m	DC block capacitor
$C_j(V_j)$	Junction capacitance at V_j
C_{j0}	Junction capacitance at zero bias
$C_f(V_f)$	Ferroelectric capacitance at V_j
C_{f0}	Ferroelectric varactor capacitance at zero bias
C_s	Sensor capacitance
$\boldsymbol{D}(\boldsymbol{\theta})$	Jacobian matrix
E	Young's modulus
f_1, f_2, f_{RF}	Carrier frequency
f_Δ	Difference frequency, $f_\Delta = f_1 - f_2$
f_{RF}	Carrier resonance frequency
f_{IM}	Intermodulation frequency, $f_{IM} = 2f_1 - f_2$
g	Gravitational force
G_r	Reader antenna gain

G_s	Sensor antenna gain
I_f	Current across the ferroelectric varactor at frequency f
$\boldsymbol{J(\theta, R)}$	Fisher information matrix
k	Boltzmann's constant
K	Effective spring constant term
L	Inductance
$l(\boldsymbol{\theta} \mid \boldsymbol{y})$	a likelihood function
L_g, L_q	Inductance of circuit
m	Mass of the sensor
P_{in}	Input power of the sensor
P_{IM}	Power at the intermodulation frequency
P_n	Noise power
q	Elementary charge
Q_m, Q_d, Q_s	Quality factor at low resonance circuit of C_m, diode and sensing element
R_a	Antenna radiation resistance
$\Re(A'), \Im(A'), \Re(B'), \Im(B')$	Real part and imaginary part of A' and B'
R_j	Diode resistance
R_g	Antenna resistance
R_f	Resistance of the ferroelectric varactror
R_q	Resistance of quartz crystal
R_s	Junction resistance at zero bias
S_{gj}	Scatter parameter from antenna to mixing diode
S_{jg}	Scatter parameter from mixing diode to antenna
S_{im}	Scatter parameter of intermodulation response
V_a	Input voltage across antenna
V_{A,RF_Δ}	Voltage received by the reader at the intermodulation frequency
V_g	Voltage across antenna
V_f	Generated voltage at one frequency
$V_{2f_1-f_2}$	Voltage at intermodulation frequency
V_n	Complex white noise
$V_g(\omega_{IM})$	Voltage across antenna at ω_{IM}
Y_j, Y_m, Y_q	Admittance of the diode, C_m and the quartz crystal
Z_n	Impedance across the diode junction
$Z_{res}(f_\Delta)$	Impedance of the resonator

1. Introduction

1.1 Motivation and Scope

The Internet of Things, or IoT, defined as “a worldwide network of interconnected objects uniquely addressable, based on standard communication protocols”, offers state-of-the-art networks of devices, systems, and services [1]. In this concept, data can be transmitted automatically over a network of things, machines, and even animals and people, without a need for human interaction between computers. Without requiring human-to-human or human-to-computer interaction, dynamic data can be transferred automatically over a network cooperatively with each other by any objects, animals, or people.

Wireless Sensor Networks (WSN) are one of the most important elements in the IoT. Wireless sensor networks (WSN) consist of networks of tens to thousands of devices, also called “sensor nodes”, which are utilized to monitor physical or environmental parameters and communicate wirelessly with a central host [2], [3]. Common monitored parameters vary from temperature, pressure, strain, humidity, and speed to positioning, proximity, vibration, and light intensity [4]–[7]. Markets for WSNs consist of process and industrial control, home and building automation, as well as safety and health monitoring. A rapid growth of WSNs from $ 0.45 billion in 2012 to $ 2 billion in 2022 is forecast in the latest market report [8]. This market growth is enhanced by the penetration of smart sensors based on microelectromechanical systems (MEMS) technology, which enables smaller size, and cost efficiency, with lower computing resources needed compared to traditional sensors [9], [10].

One way to establish a wireless connection is by using a radio transceiver. Radio transceivers, however, require an energy source, such as a battery

or an energy harvester in the wireless node [11], [12]. Therefore, the lifetime and operation conditions may be limited, not to mention the added cost, complexity, and size required.

In some cases, the need for an energy source in wireless devices can be avoided by using passive wireless sensors with an active reader. In this approach, the communication between a sensor and reader is established by applying modulated backscattering [13]. In this technique, a passive sensor is actuated by an electromagnetic signal transmitted by the reader, and the sensor communicates back to the reader by reflecting a portion of the interrogation signal.

Typical types of passive wireless sensors include RF-identification (RFID) [14], [15], surface acoustic wave (SAW) sensors [16], near-field coupled electrical resonance circuit sensors [17], and harmonic sensors [18]. However, these methods have several limitations, confining the applications where sensors are feasible. For instance, they only provide a relatively short detection distance and are expensive.

The objective of this dissertation is to develop a passive wireless sensing technology that can overcome the limitations of the existing passive wireless sensors. In particular, the developed sensing technologies should offer a long read-out distance and facilitate a generic sensing element. To address these challenges, the so-called intermodulation communication principle for wireless sensors is developed further in this dissertation. In this concept, the sensor comprises an antenna, a mixing element, a low frequency resonance circuit, and a generic sensing element. In this dissertation, the sensor platform is optimized and developed for different applications, a frequency-based identification with the new sensor is demonstrated, and an advanced data analysis method is applied to estimate the sensor state.

1.2 Scientific Contribution

The scientific contributions in this thesis are the following:

1. A new passive wireless sensor platform based on the intermodulation communication principle is presented. The analytical equations for predicting the intermodulation response of the sensor are elaborated. The sensor offers long read-out distance and narrow bandwidth. The platform utilizes a mechanical resonator, enables an ID-code to identify the

sensor and the use of a generic sensor element. [I]

2. The intermodulation communication principle is used in passive wireless sensors. Optimization of the sensor structure is proposed in order to obtain long read-out distance and good resolution. The optimization theory and design equations for this purpose are presented and optimization of the electrical circuitry is carried out. The optimization theory is verified by harmonic balance simulations and experiments as well. [II]

3. In the intermodulation communication principle, the sensor value is estimated from the analog sensor response, which always contains noise. Moreover, the relation between the sensor state and the response is nonlinear. Due to these reasons, the sensor state estimation is a challenge. A signal model for the intermodulation communication principle is developed and the derived signal model is later used by Dr. Jussi Salmi to estimate the quantity measured by the wireless sensor from its intermodulation response. The algorithm is experimentally verified with a passive wireless inclinometer sensor at 860 MHz. [III]

4. A frequency division concept for intermodulation communication sensors is introduced and realized. In this concept, each sensor replies to the reader at different intermodulation frequencies. It enables the use of multiple identification codes (IDs) and multiple access protocols when several sensors are within the reading range of one reader. [IV]

5. Intermodulation sensors enable the use of generic sensing elements, meaning that sensors can potentially make the concept suitable for many applications. Examples have already appeared in the literature. The intermodulation communication principle for sensing is experimentally demonstrated in the application of electrocardiography ECG, and in inclinometer and accelerometer measurements. [V][VI]

6. A novel integrated passive device (IPD) process is applied in order to integrate the passive components of a passive wireless sensor platform. The possibility of realizing a highly integrated sensor in the IPD process is experimentally studied. The concept is validated with a MEMS accelerometer sensor used to measure the sensor's inclination in a static gravitational field. [VII]

7. Several approaches have been proposed to realize the intermodulation sensor. A comprehensive comparison of different passive wireless sensors based either on a mechanical resonator and an electrically nonlinear sensing element, or a separate mixer, a low-frequency resonance circuit, and a sensing element is carried out. The comparison helps to understand different architectures and their benefits and drawbacks.[VIII]

8. A novel system architecture combining passive wireless intermodulation sensors and their associated reader is proposed. The proposed reader architecture can provide high power levels and meet frequency regulations in UHF RFID sensor systems [IX]

2. Passive Wireless Sensors

Passive sensors do not require batteries. They do not require any power source other than the electromagnetic energy from the reader device. Therefore, they are small, less complex, cheap and have long lifetime. Depending on the working frequencies, passive wireless sensors are normally classified into passive low-frequency (LF) sensors, high-frequency (HF) sensors, and ultra-high-frequency (UHF) sensors [19]. Typically, LF and HF tags have a read range of up to 1 meter [20] [21], while a simple passive UHF sensor can typically be read from 5 to 10 meters in free air [22], although, a read range of more than 35 meters can be achieved by a high performance UHF Gen 2 tag [23]. Another traditional way to classify the passive sensors is based on the operational principles. Typical passive wireless sensors are RF identification (RFID), surface acoustic wave (SAW) RFID, electrical resonance circuit sensors, harmonic sensors, and intermodulation sensors. A comparison of different passive wireless sensor technologies is summarised at the end of the chapter.

2.1 RFID

RFID is an identification technology which utilizes electromagnetic waves to transfer information between tags and readers. It has replaced barcodes in many applications. The benefits of RFID are that it does not require optical line-of-sight and hundreds of RFID tags can be read at a time [24].

A generic passive RFID tag is composed of an antenna and an application-specific integrated circuit (IC) chip, which enables several advantages such as identification, rewritable memory and anti-collision protocol [25]. RFID utilizes modulated backscattering [13] to transfer the stored identification information to the reader. Fig. 2.1 illustrates the modulated

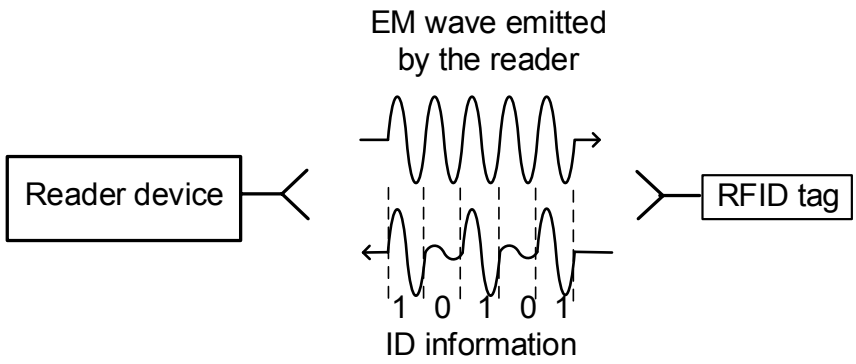

Figure 2.1. Backscattering communication principle in a RFID system. IDs are backscattered to the reader as a modulated signal when the tag is illuminated by the reader.

backscattering principle. When illuminated by a RFID reader, the tag antenna rectifies the power from the RF signal emitted from the reader device. The rectified power is applied to start up the IC chip. The transmitted RF signal is modulated by the identification information in the IC chip and then backscattered. The modulation in the backscattered signal is recorded by the reader antenna which interprets the information. The highest read out distance is limited by the power needed for the integrated circuit (IC) and is typically 5–10 m [22].

RFID was initially used for identification and is increasingly used for other purposes such as localization and items tracking [26]. RFID has been used in many fields, from agriculture [27], [28] to industry [15], [29]. For instance, it is widely utilized in industrial automation applications due to its relatively large information capacity, long read out distance, high read-out accuracy, and good mechanical robustness. For example, RFID can be used in the paper industry to identify individual paper and board reels throughout their life cycle [30]. RFID attached to an automobile can be used for body tracking in the manufacturing procedure [31].

The focus for developing RFID has mainly been on identification [32], but has increasingly moved towards other possible applications such as on sensing [33]. RFID can be equipped with digital sensors or analog sensors. When used with digital sensors, an A/D converter, a microprocessor or other digital logic, and a sensing element are added to the RFID tag [34]– [37]. By doing this, analog sensing data is sampled in digital format and transmitted back to the reader. This method enables the use of generic sensor elements, which broadens possible range of applications.

However, the additional elements further increase the power consumption and shorten the read-out distance. For example, a 3 m read–out distance is achieved with the approach in [38], whereas the read-out distance of a tag without a sensor element is typically 5–10 m.

Sensing can also be realized with an analog approach [39]–[42] in which, an antenna is loaded with a sensing element or a material whose electrical properties are sensitive to the measured quantity. The sensor element or material affects the antenna matching and impedance tuning the operation frequency. Hence, the sensing data is modulated into the operating frequency and can be retrieved by recording the shifting of the operating frequency or by recording the strength of the reflected signal at one frequency. Alternatively, the sensed quantity can be obtained with a self-tuning chip which contains a tuning element to compensate for the changed impedance due to sensor [42]. The advantage of this approach is that a relatively long distance compared with digital sensing can be achieved for the reason that the sensing element is one part of the matching network which does not necessarily increase the power consumption. However, this approach requires the sensing elements to operate in the microwave range, while most of the sensing elements on the market are designed to operate below a few MHz. Sensitive materials go higher in frequency but may lack sensitivity or selectivity or otherwise be suboptimal for sensing purposes. Moreover, there are many other factors affecting the antenna matching and impedance. For instance, antenna impedance in free space is obviously quite different from that when the antenna is close to conductive or dielectric objects.

2.2 SAW Sensors

SAW tags have been available for more than 30 years. SAW sensors can operate in harsh environments [43]. SAW tags use a time modulation, where the ID is coded into the time delays of reflections. SAW tags are linear, time-invariant systems. A SAW delay line is applied in the reader to separate between the request and the response signals. Limited by the signal-to-noise ratio, as well as by the largest allowed radiation power, the read range of SAW tags can be up to several meters [44]. They are purely passive, and reflect and re-emit the request. SAW tags have a simple structure compared with IC-RFID. Moreover, SAW tags operate as delay lines and provide a sufficient delay since they apply surface acoustic

waves which are 100,000 times slower than EM waves [44].

The operation principle of a surface acoustic wave (SAW) sensor is based on converting an interrogating radio wave from the reader directly into a nano-scale surface acoustic wave on the surface of a piezoelectric substrate [16].

A typical SAW sensor is composed of a transponder antenna and a SAW Chip which consists of an interdigital transducer (IDT) and an array of reflectors on a piezoelectric substrate. The operation principle is illustrated in Fig. 2.2. The antenna receives an electromagnetic (EM) signal from the reader device and the inter-digital transducer (IDT) transforms the electric field into a surface acoustic wave that is propagated on the piezoelectric material. The generated mechanical pulse then propagates over the surface of the piezoelectric crystal. The SAW pulse is partly reflected and partially transmitted by the reflectors. These reflectors are precisely placed on the substrate. and the reflected acoustic wave contains the coding information on the positions of the reflectors. The reflected pulses are further converted back into the electromagnetic field at the interdigital transducer (IDT) and emitted back to the reader device by the transponder antenna. By recording the time delays of the reflected pulses, a tag with an ID can be realized. The encoding method is known as time position encoding or pulse position modulation (PPM) [44].

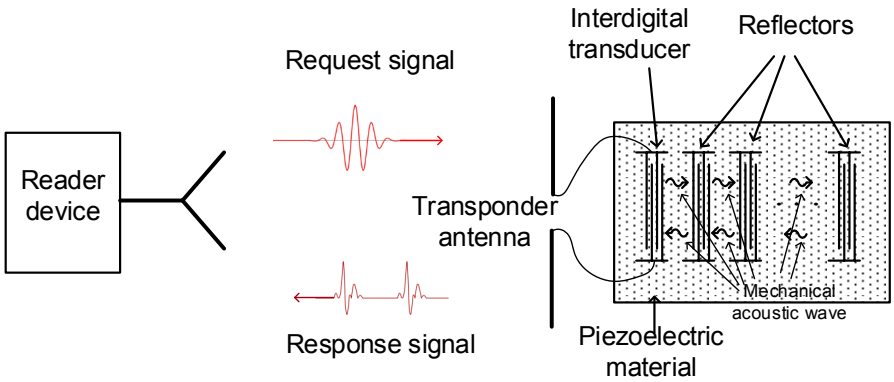

Figure 2.2. Operation principle of the SAW tag. Response signals are the delays of the request signals by the reflectors.

Quartz (SiO_2), lithium niobate ($LiNbO_3$), and lithium tantalate ($LiTaO_3$) are commonly used piezoelectric materials. The SAW propagation properties of the piezoelectric material (e.g. velocity) depend on the physical and chemical quantities such as temperature or pressure. A change in the

reflected acoustic wave can be detected making the sensing possible. SAW sensors have been available for decades, and have been used in many applications [45] such as in the non–contact measurement of temperature [46], pressure [47], [48], torque [49], and bending [47]. High sensitivity and intrinsic reliability are the benefits of SAW sensors. Still, the relatively large size, short read–out distance due to high acoustic loss [50], and high inherent fabrication costs limit their applicability in some cases. Furthermore, the operation frequency (up to several gigahertz) of SAW sensors is limited by the line of the IDT structure. SAW tags only provide hard-coded identification (ID) which is determined by the positions of the reflectors.

2.3 Resonance Sensors

Resonance sensors are composed of a resonator, a reactive coupling element, and a sensing element whose capacitance, inductance, or resistance changes according to an environmental parameter. A schematic circuit of a typical resonance sensor and a coupled reader device are shown in Fig.2.3. The sensor in the figure is a RLC-resonator, whose inductance or capacitance (L_3 and C_2 in Fig. 2.3) is sensitive to a physical quantity and therefore also affects the resonance of the sensor [17], [51]. The reader device obtains the state of the sensing element (i.e capacitance) by measuring the impedance of the RLC-resonator. The main weakness of this

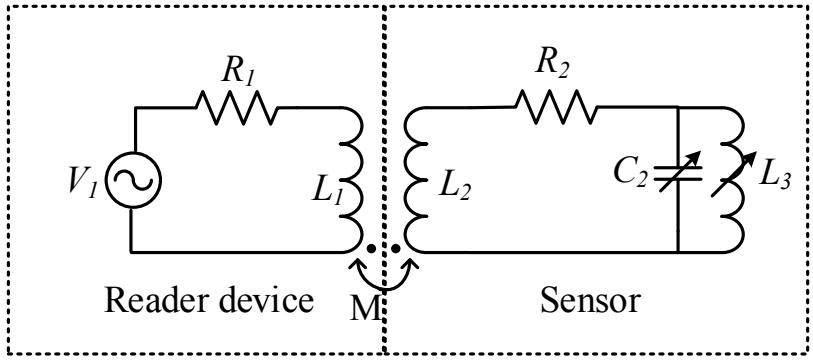

Figure 2.3. Electrical equivalent circuit for the inductively coupled electrical resonance-circuit sensor.

technology is that the read–out distance cannot be long because of the need of near–field coupling (M in Fig. 2.3) to the reader device. Another limitation of resonance sensors is that their resonance may be affected by proximity to conductive or dielectric objects [52]. This kind of sensor has

been utilized to measure strain [17], pH [53], and moisture [54].

2.4 Harmonic Sensors

The operation of harmonic radars and tags is based on the frequency conversion of the tag in which the sensor is composed of an antenna and a non-linear element [18]. Ideally, the antenna should be matched to the non-linear element at the fundamental frequency and at the used harmonic frequency to enable efficient frequency conversion. Non-linear elements are applied to generate the harmonic frequencies. When the sensor is activated by the reader with the fundamental tone, the sensor generates and replies with signals at the harmonic frequencies. The reader can transmit a single or multi-tone signal. In the case of a single tone f_1, the sensor replies at nf_1 [18]. It can also be formed by signals at multiple frequency components. For example, with f_1 and f_2, the sensor replies at the harmonic frequencies $nf_1 \pm mf_2$ [55], [56]. The operation in both cases is shown in Fig. 2.4.

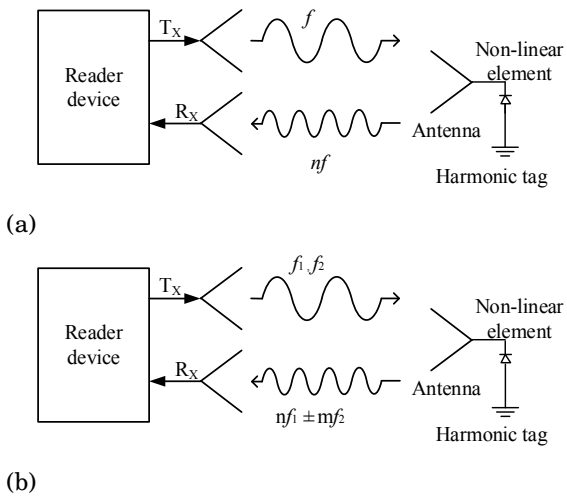

Figure 2.4. Operation of harmonic sensors for cases: (a) with one input frequency component, (b) with two input tones.

Generally, the non-linear element can be a diode, a varactor or a MEMS (Microelectromechanical systems) resonator. The harmonic sensors are typically passive, i.e. they only use the energy of the received electromagnetic waves. Although most harmonic sensors operate at microwave frequencies, a partly optically actuated sensor is proposed for accurate spatial localization [57].

Harmonic radar systems have been mainly used for localization of objects. Harmonic sensors were initially developed for automotive vehicles [58], [59] and can provide a good performance for target tracking in a high clutter environment [60]–[62]. They have been used to track insects for 20 years [61]–[67]. For example, they are reported to provide an effective modality for tracing insect behavior [62]. Moreover, harmonic radar and tags can also be used to find avalanche victims [68], [69].

Harmonic tags can also be made suitable for sensing purposes. Embedded harmonic tags have been developed to monitor the health of civil infrastructure such as bridges and overpasses [70], [71]. It is also possible to apply a sensing element in parallel with the non-linear element. In [72], it is claimed that the capacitive sensor information can be monitored wirelessly by observing the phase of the reflected harmonic signal. Temperature is reported to be monitored by placing a temperature-dependent bandpass filter before the non-linear element [73].

In general, harmonic tags can be used at high frequencies and can provide large read-out distances. However, the concept in Fig. 2.4.(a) replies at the harmonic frequencies, which does not comply with the frequency regulation.

A comparison of different passive wireless sensor technologies is summarised in Table 2.1.

Table 2.1. Comparison of different passive wireless sensor technologies

Type	Principle	Advantages	Read Range	Application	Sensing possibility	ID possibility	Limitation
RFID	Modulated backscattering	ID, Rewritable memory anti-collision protocol	5-10 m	Identification localization, tracking,	Yes (Digital Sensor, sensitive material in antenna)	Yes	Shorter distance with a sensing element
SAW	Coverting between EM wave and acoustic wave	High sensitivity intrinsic reliability	Several meters	Temperature Pressure	Yes (Piezoelectric substrate)	Yes	High acoustic loss, high fabrication costs
Resonance sensor	Near-field coupling	Durable	Several centimeters	Strain, pH, moisture	Yes (Capacitive, inductive sensor)	No	Short range, Sensitive to surroundings
Harmonic sensor	Frequency conversion	Long read range	More than 10 m	Localization, sensing	No	Yes	Some do not comply with frequency regulations

3. Intermodulation Communication Principle and Its Sensor Applications

In recent years, the intermodulation communication principle has been developed for passive wireless sensors [74]–[77]. For example, it has been used to measure the distance of the tag to the sensor in [74]. The intermodulation sensor is a subset of harmonic sensors. Unlike the normal harmonic sensors in Fig. 2.4(a) which transmit one tone f_1 and receive a signal at the second harmonic $2f_1$, intermodulation sensors are actuated by two tones, f_1 and f_2, and they produce the intermodulation frequency $2f_1 - f_2$, $2f_2 - f1$. An advantage of intermodulation sensors is that they can be made compliant with frequency regulations because all the frequencies are closely located and can be fitted into one band. Moreover, compared to other passive wireless sensor techniques, such as RFID, SAW, and near-field coupled resonance sensors, sensors based on the intermodulation principle can provide relatively high accuracy across a large read out range (up to tens of meters), and enable the possibility to utilize a generic sensor element.

3.1 Intermodulation Communication Principle

In the intermodulation communication principle (see Fig. 3.1), the reader transmits signals containing two closely located frequencies, f_1 and f_2. Once the signals are received by the sensor, it generates signals at the harmonic frequencies $nf_1 \pm mf_2$ due to the non-linearity of the sensor circuitry. These frequencies are further backscattered to the reader. The sensor is constructed in such a way that the signal at an intermodulation frequency depends on the sensor parameter. Hence, by recording the intermodulation response as a function of frequency, the sensor information can be obtained. In principle, all intermodulation frequencies can be used to carry the sensor information. Lowest order modes, $2f_1 - f_2$ and

$2f_2 - f_1$ are typically the strongest and therefore best suited for communication. If possible, it best use both side bands simultaneously to achieve the strongest response. If the reader hardware allows to record only one of them, it does not matter which one of the side bands is selected as both are equally strong.

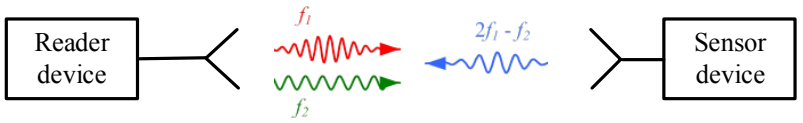

Figure 3.1. Intermodulation read–out principle. The reader transmits two tones and the sensor replies at an intermodulation frequency.

3.2 Sensor Architectures

There are several alternative ways to realize a passive wireless sensor based on the intermodulation operation principle. In its simplest form, a sensor can consist of one antenna and another component such as a resonant MEMS sensor, an electrically non-linear sensor, or a mixer and sensing elements. Some presented architectures are reviewed in the following sections.

3.2.1 Sensors Based on Resonant MEMS

The simplest intermodulation sensor is composed of one antenna matched directly to a capacitive MEMS resonator. Fig. 3.2 shows the architecture and its simplified electrical equivalent circuit.

When the sensor is activated by the reader at two closely located frequencies f_1 and f_2, a voltage at the same frequencies is induced across the MEMS cantilever. Because of the non-linearity of the capacitive actuation, forces at all harmonic frequencies, $nf_1 \pm mf_2$ (n, m are integers), will be generated. The frequency difference $f_1 - f_2$ is selected to be equal to the resonance frequency of the cantilever, causing oscillation at that frequency.

The displacement of the cantilever from its initial position will change the capacitance of the MEMS resonator. In this way vibrations cause a modulated reflection. Due to the modulation, the device reflects signals at the intermodulation frequencies $2f_1 - f_2$ and $2f_2 - f_1$. The reflected voltage

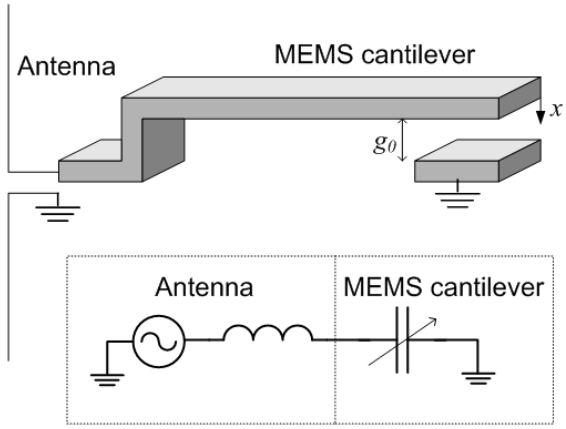

Figure 3.2. Schematic principle of an intermodulation sensor based on a resonant MEMS sensor (top) and its equivalent electrical circuit (bottom). The Figure is not to scale [VIII].

$V_{2f_2-f_1}$ at one intermodulation frequency is proportional to the mechanical properties of the MEMS resonator. Hence, by reading the intermodulation response at the reader side, the displacement of the cantilever will be recorded [75].

One advantage of this kind of sensor is its simple architecture. However, the sensor element (MEMS resonator) needs to operate at microwave frequencies. This requirement may prevent the exploitation of commercially available sensors.

3.2.2 Sensor Based on Electrically Non-linear Sensor Element

Another approach involves utilizing an electrically non-linear sensor element. Examples of the suitable elements include: a ferroelectric varactor exhibiting a voltage-dependent capacitance, a photodiode that is sensitive to light, a varactor diode for voltage measurements, and a microbolometer for temperature or strain monitoring purposes. Here, the sensor utilizing a ferroelectric varactor is given as an example.

Consider a ferroelectric varactor matched to an antenna, as shown in Fig. 3.3. When illustrated by a signal consisting of two closely located frequencies, the sensor antenna generates a voltage across the ferroelectric varactor. The generated voltage V_f is determined by the quality factor Q of the ferroelectric varactor and the reflection coefficient Γ of the antenna and the varactor, and the input voltage across the antenna V_a

$$V_f \sim Q(1 - |\Gamma|)V_a. \tag{3.1}$$

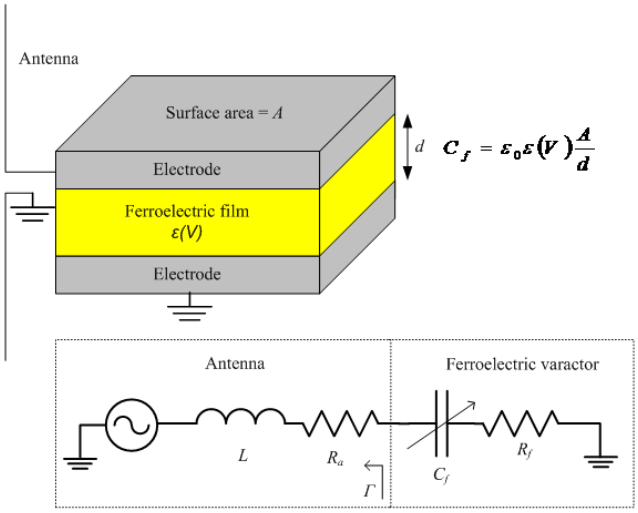

Figure 3.3. A schematic layout of a wireless sensor based on a ferroelectric varactor (top) with the equivalent circuit model (bottom). The figure is not to scale [VIII].

The capacitance of a ferroelectric varactor is a symmetric function of the voltage and can be approximated as

$$C_f(V_f) \approx C_{f0} + C_f{}' {V_f}^2, \tag{3.2}$$

where C_{f0} is the capacitance at zero-bias and $C'_f {V_f}^2$ is the capacitance change due to the voltage across the ferroelectric varactor. As a result, the current across the varactor is calculated as

$$I_f \approx j\omega(C_{f0} + C'_f {V_f}^2)V_f = j\omega C_{f0} V f + j\omega C'_f {V_f}^3. \tag{3.3}$$

The first term in (3.3) represents linear currents and the second term contributes to intermodulation products. The reflected signal at the intermodulation current is obtained by solving the voltage across the radiation resistance at the intermodulation frequency. Eventually, the reflected voltage at one intermodulation frequency is proportional to

$$V_{2f_2-f_1} \sim Q^4(1 - |\Gamma|)^4. \tag{3.4}$$

As the capacitance at zero-bias of a ferroelectric varactor C_{f0} depends on temperature and the zero-bias capacitance affects the reflection coefficient between the antenna and the varactor, the temperature can be obtained by measuring the intermodulation response of the sensor as a function of the frequency. Therefore, the capacitance and the temperature can be

calculated by fitting the measurements to the following model:

$$\Gamma = \frac{R_f + \frac{1}{j\omega C_f} - R_a + j\omega L}{R_f + \frac{1}{j\omega C_f} + R_a + j\omega L}, \tag{3.5}$$

where R_f, R_a,L, and C_f are shown in Fig. 3.3 as the varactor resistance, antenna radiation resistance, antenna matching inductance, and varactor capacitance, respectively. This sensor architecture is extremely simple, enabling the possibility to realize fabrication processes capable of printing ferroelectric materials using printed-electronics. A drawback with the approach comes from the relatively broad frequency response which does not allow good identification. Moreover, as the antenna is part of the sensor circuitry, environmental loading of the antenna causes uncertainty to the sensed quantity.

3.2.3 Sensors Based on Mixer and Low-frequency Resonance Circuits

The previously discussed intermodulation sensors utilize the same element (MEMS or ferrovaractor) simultaneously for mixing and sensing. As commercially available sensors do not typically mix microwave frequencies efficiently and mixers cannot typically be used as sensors, the lack of suitable components greatly limits the applicability of the intermodulation communication concepts. Moreover, if the antenna of a sensor based on an electrically non-linear sensor is in close proximity to a conductive or dielectric material, the antenna impedance and matching changes, affecting the sensor in the same way as if it had changed its value. Hence, a practical way to realize an intermodulation sensor is to separate the mixing and sensing components.

The following describes one such architecture in which the main parts of the sensor are composed of an antenna, a passive mixing diode and finally a low-frequency resonant circuit with sensing ability (see Fig. 3.4).

The intermodulation generation process is broken down into the steps shown in Fig. 3.5. The reader starts an inquiry by sending two close frequencies f_1 and f_2. Once the tones are received by the sensor antenna, these frequencies are mixed in the diode, generating currents at harmonic frequencies such as the difference frequency $f_1 - f_2$ as well as other frequencies, for example, $2f_1$, or $2f_2$. These currents at the harmonic frequencies then pass through the low-frequency resonant circuit. The currents generate a voltage that is proportional to the impedance of

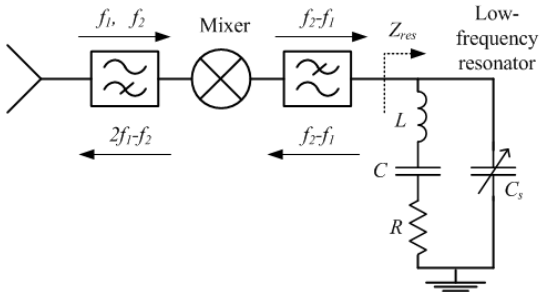

Figure 3.4. A schematic layout of an intermodulation sensor based on a separate mixer and sensing element [VIII].

the low–frequency resonance circuit. Since the low frequency resonant circuit is designed such that the resonance frequency is close to the difference frequency $f_1 - f_2$, only the voltage induced at the difference frequency $f_1 - f_2$ gets enhanced and reflected back to the mixing diode. This voltage further mixes with the original input frequencies, generating the current at the intermodulation frequency $2f_1 - f_2$. Eventually, the signal at the intermodulation frequency $2f_1 - f_2$ is back scattered to the reader by the sensor antenna. Because the voltage at the difference frequency $f_1 - f_2$ is proportional to the impedance of the low frequency resonate circuit which is directly affected by the sensing element, it contains the sensing data. This sensing data is further transferred to current at the intermodulation frequency in the mixer, and thus, the sensing data can be read out by recording the intermodulation response.

The backscattered signal at the intermodulation frequency $V_{2f_2-f_1}$ depends on the impedance of the resonator $Z_{res}(f_\Delta)$ at the difference frequency

$$V_{2f2-f1} \sim A + BZ_{res}(f_\Delta), \tag{3.6}$$

where A is the intermodulation signals caused by other components in the circuit and B shows the scale of the intermodulation signal due to the impedance of the resonator $Z_{res}(f_\Delta)$.

For a low frequency series RLC resonant circuit in parallel to a sensing element whose capacitance depends on some physical or environmental parameters (shown in Fig. 3.5), the impedance at the difference angular frequency, $\omega_\Delta = 2\pi(f_1 - f_2)$, can be calculated as

$$Z_{res}(f_\Delta) = (j\omega_\Delta C_s + \frac{1}{R + j\omega_\Delta L + 1/(j\omega_\Delta C)})^{-1}, \tag{3.7}$$

where R, L, and C come from the low frequency resonator and C_s represents the sensing element. Note that the difference frequency can be very

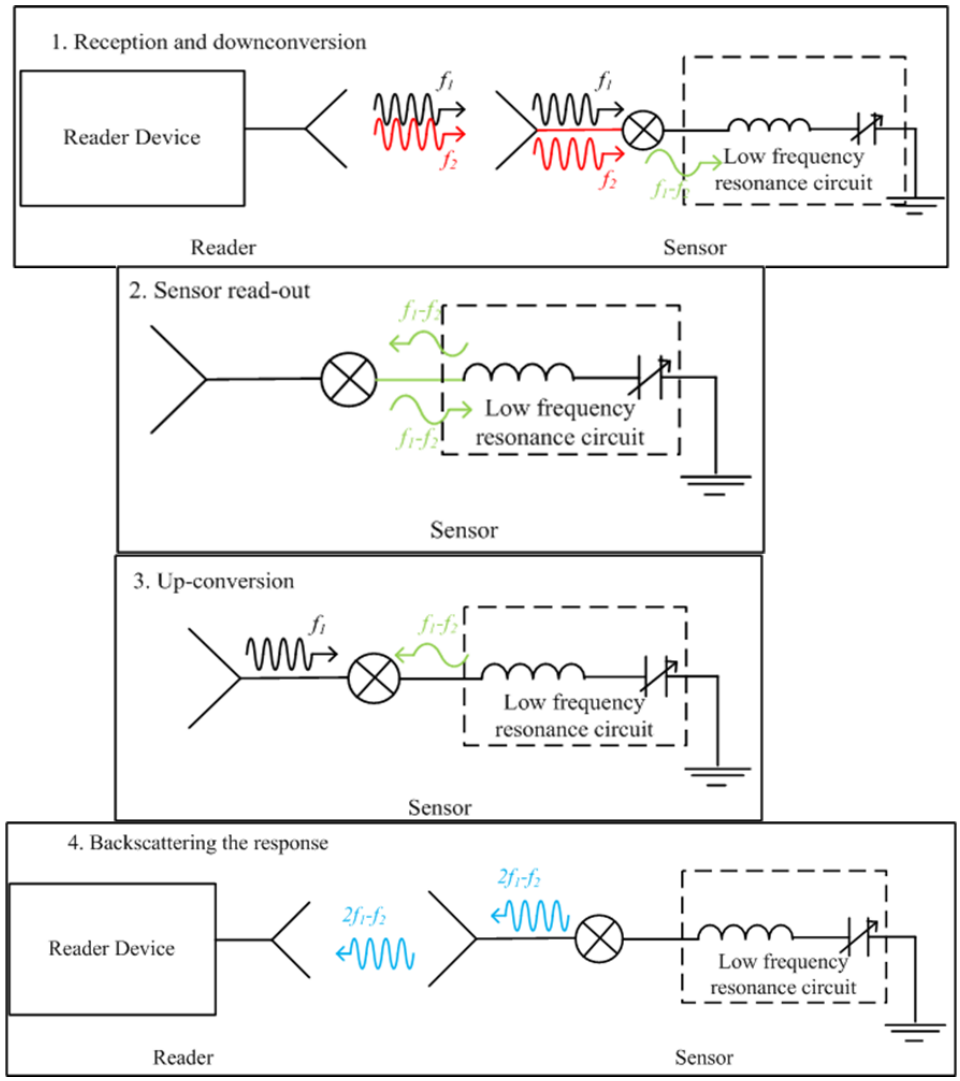

Figure 3.5. Intermodulation communication principle for a sensor based on a mixer and a low frequency resonance circuit.

low (in the order of 10 kHz to 10 MHz) and thus facilitates the use of most commercially available sensors.

The low frequency resonator determines the sensitivity and the tuning range of the sensing element. In general, the resonator should provide both a high quality factor and large tunability. Mechanical resonators, as compared to their electrical counterparts, provide a narrower bandwidth, a higher quality factor, and greater equivalent inductance for a given self-resonant frequency. Therefore, a sensor based on the mechanical resonator enables a larger read-out distance and a smaller frequency offset which facilitates compliance with frequency regulations.

3.3 Design Considerations for An Intermodulation Sensor

There are many components in a sensor that need to be matched together in order to provide a large read out distance and good measurement resolution. The following considers design choices for these parts.

Given the above three alternatives, it is easy to understand that a sensor based on mixer and a mechanical resonator is the best structure to form a intermodulation sensor as it facilitates the use of generic sensing elements.

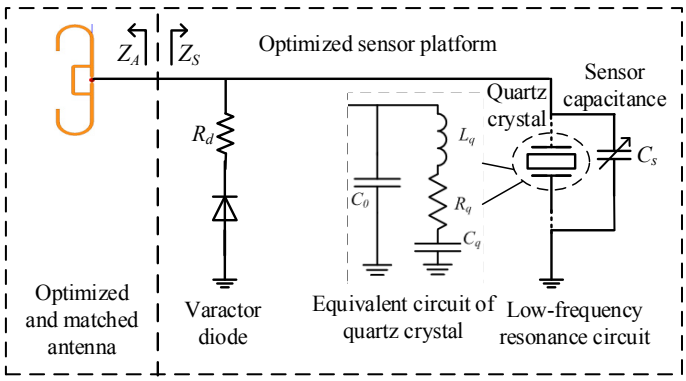

Figure 3.6. The sensor structure consists of a matched antenna, a mixer diode, and a mechanical resonator with a sensor element.

Let us consider a sensor structure composed of an antenna, a mixer diode, and a mechanical resonator in parallel with a sensing capacitor as shown in Figure. 3.6. A simplified electrical equivalent circuit of such a sensor is shown in Fig. 3.7. The matched antenna is represented by a voltage source $V_{g,\omega_{IM}}$ with a radiation resistance R_g in series with the

matching component L_g, R_i represents the loss of L_g, and C_m is used for DC blocking. The mixer is modeled as a tunable capacitor C_j with resistance R_d, and the mechanical resonator is simplified as a series RLC resonator in parallel with a capacitor C_0. C_s is the sensing element and R_s is its resistance. A low pass filter (shown between the diode and capacitive sensor in Fig. 3.7) is needed in order to prevent the RF frequencies from entering the low-frequency resonance circuit. Let us consider the equivalent circuit shown in Fig. 3.7.

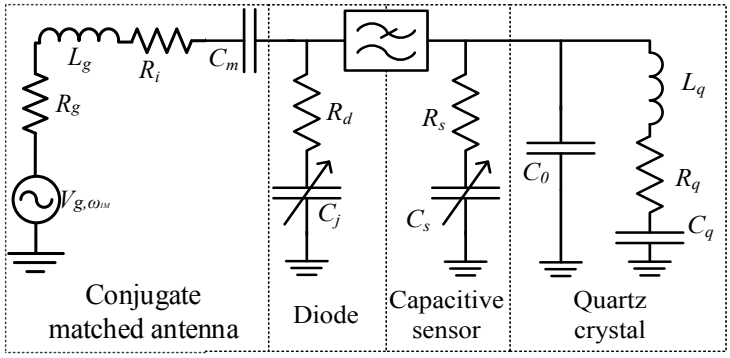

Figure 3.7. Equivalent circuit for the optimized sensor.

The normalized backscattered voltage at the intermodulation frequency $V_{g,\omega_{IM}}$ from the sensor is obtained as [II]:

$$\frac{\widetilde{V}_{g,\omega_{IM}}}{\sqrt{R_g}} = 4P_{in}^{3/2}R_g S_{jg}^3(\omega_{RF})Z_n(\omega_{RF})S_{gj}(\omega_{RF})[\frac{\alpha}{2R_j} + \frac{j\omega_{RF}C_{j0}\gamma(\gamma+1)}{2\Phi^2} - \frac{\omega_{RF}^2 C_{j0}^2\gamma^2 Z_n(2\omega_{RF})}{2\Phi^2} + (\frac{\alpha}{R_j} + \frac{j\omega_\Delta C_{j0}\gamma}{\Phi})\frac{j\omega_{RF}C_{j0}\gamma Z_n(\omega_\Delta)}{\Phi}], \tag{3.8}$$

where P_{in} is the received power at each frequency, R_g is the antenna impedance, $S_{jg}(\omega_{RF})$ is the voltage transfer function from antenna to the junction of the diode, $S_{gj}(\omega_{RF})$ is the voltage transfer function from the junction of the diode to the antenna, $\alpha = q/nkT$ where q is the elementary charge, n is the ideality factor, k is the Boltzmann's constant. T is the temperature, $R_j = 1/\alpha I_s$ is the junction resistance at zero bias, I_s is a saturation current, C_{j0} is a junction capacitance at zero bias, γ is the profile parameter, Φ is a junction potential, and Z_n is the impedance across the diode junction.

The sensor platform receives the two fundamental frequencies ω_1 and

ω_2, and replies at the intermodulation frequency $\omega_{IM} = 2\omega_1 - \omega_2$. Since the difference frequency ω_Δ is small compared to the carrier frequency that it is assumed that $\omega_{RF} \approx \omega_1 \approx \omega_2 \approx \omega_{IM}$.

Let us consider a capacitive sensor with a relative sensitivity β towards a measured physical quantity x

$$\beta_x = (\frac{\delta C_s}{C_s})/(\frac{\delta x}{x}), \tag{3.9}$$

where C_s is the capacitance of the sensor. Let us further assume that a sensor capacitance only affects $Z_n(\omega_\Delta)$ in (3.8). Considering the configuration in Fig. 3.7, obviously, the highest sensitivity can be achieved when the antenna is matched with the matching components and the diode, that is, $R_g = R_i + R_d$ and $L = (C_m + C_j)/\omega_{RF}^2 C_m C_j$. After some manipulation, the voltage change at the intermodulation frequency due to the change in the measured physical quantity is

$$\frac{\Delta\widetilde{V}_{g,\omega_{IM}}}{\sqrt{R_g}} = \frac{P_{in}^{3/2}}{4} \frac{1}{(\frac{C_j + C_m}{C_m Q_m} + \frac{1}{Q_d})^2} \cdot \frac{C_s}{(\frac{C_m}{Q_m(\omega_\Delta)} + \frac{C_j}{Q_j(\omega_\Delta)} + \frac{C_s}{Q_s(\omega_\Delta)} + R_g\omega_\Delta(C_m + C_j + C_s + C_o)^2)^2} \frac{\gamma^2}{\omega_{RF}\Phi^2} \beta_x \frac{\Delta x}{x}, \tag{3.10}$$

where $Q_m(\omega_{RF})$ and $Q_d(\omega_{RF}$ is the electrical quality factor of the matching circuit and that of the diode at RF, respectively. $Q_m(\omega_\Delta)$,$Q_j(\omega_\Delta)$, and $Q_s(\omega_\Delta)$ are the quality factors of the matching circuit, diode, and sensor at the difference frequency, respectively. According to (3.10), the read-out sensitivity can be maximized by selecting the correct capacitances when the quality factors of different components are assumed to be constant.

The sensitivity of the circuit is obtained from simulations by sweeping the difference frequency f_Δ, and by calculations using (3.10). In both cases, the highest value is normalized to 1. The calculated and simulated sensitivities as a function of C_s is shown as one example in Fig. 3.8.

Fig. 3.8 shows that the calculations predict similar sensitivity behavior as the simulations. According to both simulations and calculations, there are optimal values for each of the components. The optimal component values in one particular case are shown in Fig. 3.9. The values have been rounded to the closest available component values. The components are arranged symmetrically in this circuit such that the sensor can be easily

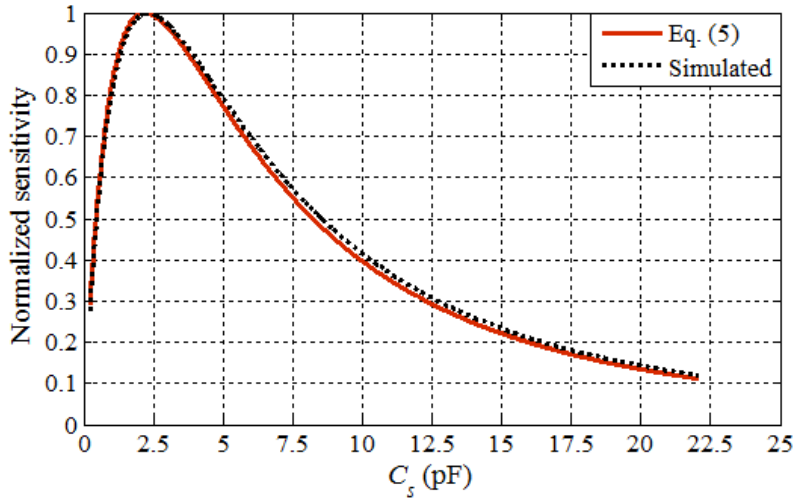

Figure 3.8. Calculated and simulated normalized sensitivity as a function of C_s [II].

matched with a dipole antenna.

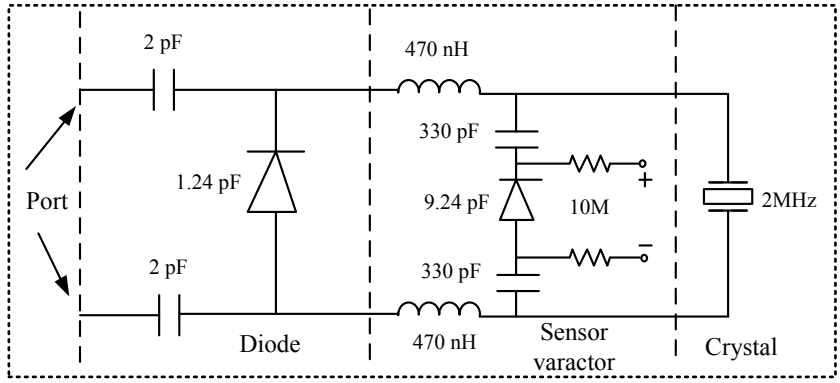

Figure 3.9. Circuit topology and tuned component values for one intermodulation sensor based on a 1.24 pF varactor and a 2 MHz crystal as mixing and resonant elements [II].

Finally, one conjugate matched antenna [78], [79] is designed to achieve the highest sensitivity after measuring the impedance of the sensor platform. Fig. 3.10 shows the final prototype of the intermodulation sensor.

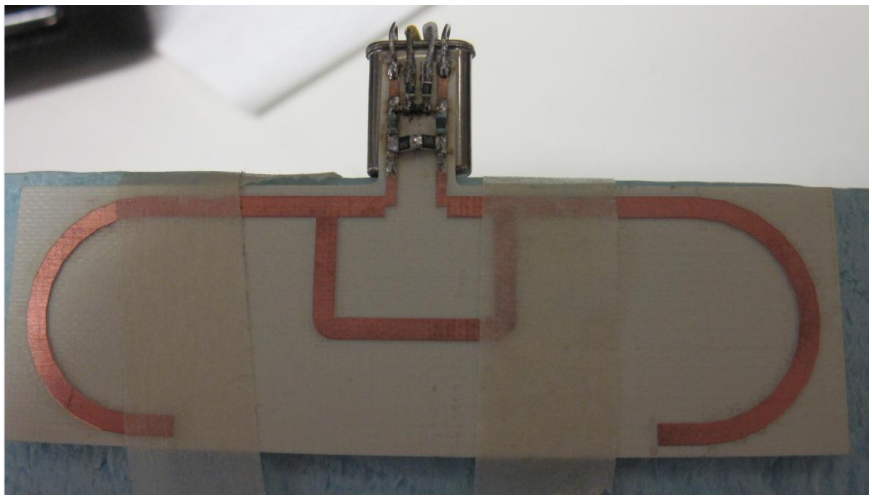

Figure 3.10. Photograph of the optimized sensor prototype [II].

3.4 Identification of Intermodulation Sensors

In practical applications, multiple sensors are often located in the same area. Identification (ID) and multiple access schemes are essential in such cases to identify the specific sensor.

3.4.1 Identification Principle

Generating IDs and implementing multiple access protocol can be straightforward in the intermodulation sensor concept. For example, IDs can be realized using distinct quartz resonators, each having a different resonance frequency. In this case, IDs are coded to the resonance frequencies. This also enables the frequency division multiple access (FDMA) concept because each sensor replies only at a specific difference frequency. Let us estimate the number of realizable IDs. Passive intermodulation sensors can be designed to fit in the European UHF RFID band (866MHz-868MHz), which means there is 2 MHz bandwidth available for IDs. If each crystal is assumed to have a relative bandwidth in the order of 10^{-5}, 460519 IDs could be realized if the lowest resonance was at 10kHz, and the highest at 1 MHz.

An alternative way to realize ID is to use varactor loaded crystals. In this approach, the intermodulation sensor can be loaded with one or multiple varactors whose capacitances can be switched between two states. This kind of ID is reprogrammable by tuning the capacitance values of the varactor.

3.4.2 Experimental Verification and Performance

The frequency–division based ID and multi–access scheme is studied with ten intermodulation sensors each with different crystals (see Fig. 3.11). The used crystal models as well as their equivalent parameters are listed in Table 3.1.

The intermodulation sensors are all equipped with switches sensitive to a magnetic field. An external magnetic field switches the sensor capacitance between “ON” and “OFF” states, resulting in the shifting of resonance frequencies. These sensors can be called binary sensors because of the on/off states

Ten intermodulation sensors reply at ten intermodulation frequencies which are well separated from each other. The resonance frequency of

Table 3.1. Used quartz crystals and their properties

Model	Resonance frequency	Co	Lq	Rq	Cq
MCRJ232000F12300H3H, MULTICOMP	32 kHz	1.15 pF	8.38 kH	19.9 kΩ	2.95 fF
X32K768L102, AEL CRYSTAL	32.768 kHz	0.75 pF	9.84 kH	20.6 kΩ	2.4 fF
CFV206 40.000KAZF-UB, CITIZEN	40 kHz	1.11 pF	5.64 kH	11.9 kΩ	2.81 fF
CFV206 60.000KAZF-UB, CITIZEN	60 kHz	1.08 pF	3.59 kH	9.1 kΩ	1.96 fF
CFV206 76.800KAZF-UB, CITIZEN	76.8 kHz	2.43 pF	2.45 MH	13.9 kΩ	1.75 fF
CFV206 100.000KAZF-UB, CITIZEN	100 kHz	0.73 pF	1.73 kH	8.31 kΩ	1.46 fF
X307K200L001, AEL CRYSTALS	307.2 kHz	9.27 pF	14.5 kH	814 Ω	18.6 fF
ECS-10-13-1H, ECS Inc.	1 MHz	5.09 pF	2.92 kH	232 Ω	8.67 fF
A-1.8432-18, IQD FREQUENCY PRODUCTS	1.8432 MHz	2.57 pF	1.09 H	239 Ω	6.82 fF
LFXTAL003037, IQD FREQUENCY PRODUCTS	2 MHz	3.16 pF	0.936 H	87.67 Ω	6.86 fF

each sensor depends on the binary state of the sensor. For example, the measured responses for both the ON and OFF states of the binary sensor at 307.2 kHz as a function of the difference frequency (as an offset from its nominal resonance frequency) are shown in Fig. 3.12. In the ON state, the resonance is much stronger and the resonance frequency higher than in the OFF state. The detailed results of the ten sensors are shown in [IV].

3.5 Practical Applications

The sensor structure based on the intermodulation communication principle might be used as a generic multi-sensing platform for different applications. Possible sensed variables include ECG (electrocardiography), binary state machines, accelerometers, inclination strains, temperature, and humidity. Several examples are given here.

3.5.1 ECG Monitoring

A wireless ECG (Electrocardiography) measurement is demonstrated with the intermodulation sensor. In this application, the intermodulation sensor is loaded with a varactor as the sensing element. The heartbeat gen-

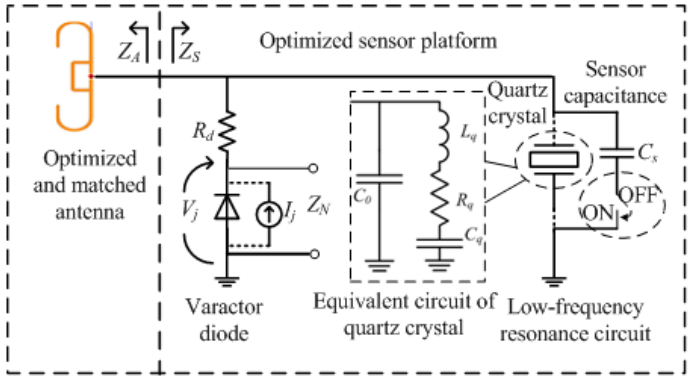

Figure 3.11. Electrical equivalent circuit of the sensor with a magnetic switch [IV].

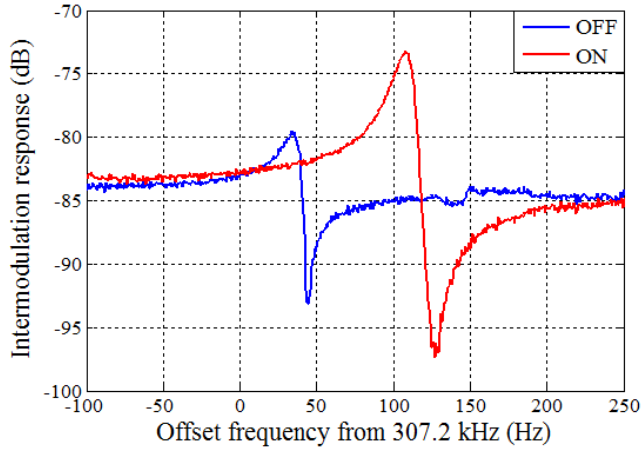

Figure 3.12. Intermodulation response of the 307.2 kHz wireless sensor in ON (red) and OFF (blue) states as a function of the difference frequency.

erates a small voltage on the skin of the chest (several millivolts), which changes the capacitance of the varactor and consequently, the output of the intermodulation response.

Fig. 3.13 shows the ECG measurement setup. The sensor is located in the anechoic chamber, and two copper patches are attached to the human body near the heart. The electric potential due to the heart's muscular activity biases a varactor which is used as a capacitive sensing element. The intermodulation response is read out in the time domain so that the heartbeat is recorded directly.

Fig. 3.14 illustrates the ECG signal of the author over a period of 60 seconds. It also slows variations due to respiration and other muscular activity.

HRV (Heart Rate Variability) is a physiological phenomenon where the time interval between heart beats varies. HRV is found to correlate with

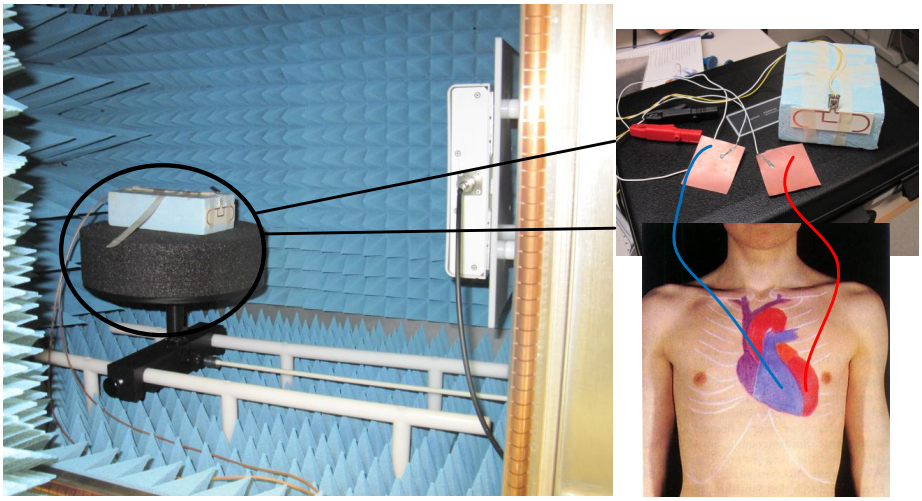

Figure 3.13. ECG measurement setup [V].

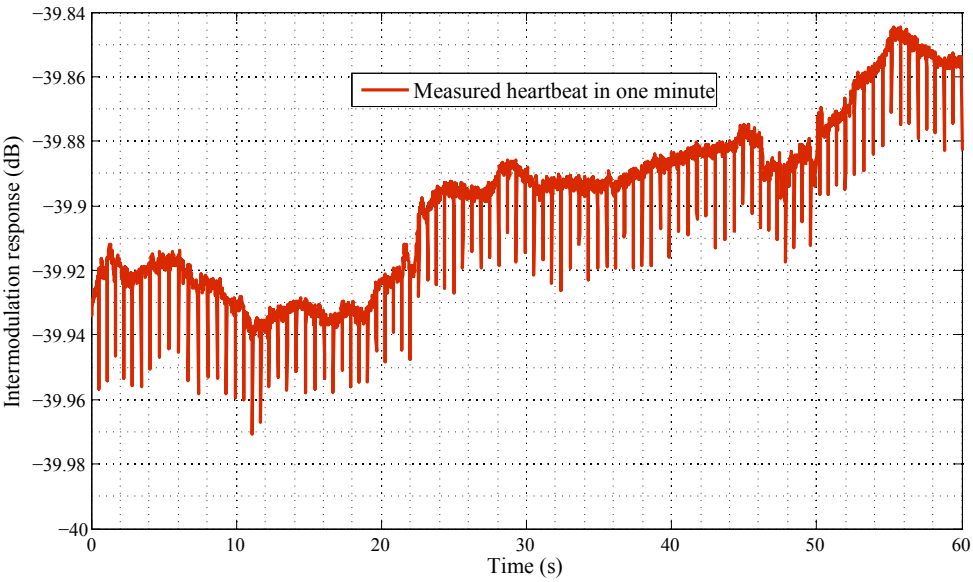

Figure 3.14. Measured heartbeat in one minute [V].

physical and mental stress. It is used also to predict or detect heart-related diseases. HRV can be calculated as the variation of the time interval between heartbeats, which is shown in Fig. 3.15. The demonstration suggests that the sensor might be used for ECG–monitoring.

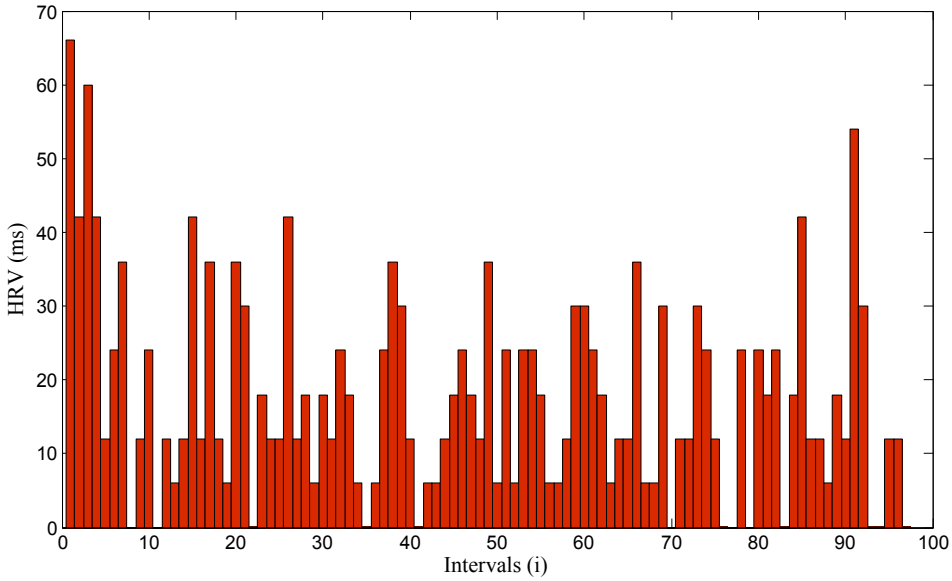

Figure 3.15. HRV signals in one minute [V].

3.5.2 Binary Magnetic Sensor

The sensor platform can be utilized as a binary magnetic sensor by using magnetically actuated switches as a sensor element. Measurements to monitor the state of the switches can be carried out in the frequency domain as well as in the time domain. Fig. 3.12 shows the intermodulation response in the frequency domain and Fig. 3.16 shows it in the time domain. One potential application could be that a sensor monitoring the state of a switch mounted on the ceiling.

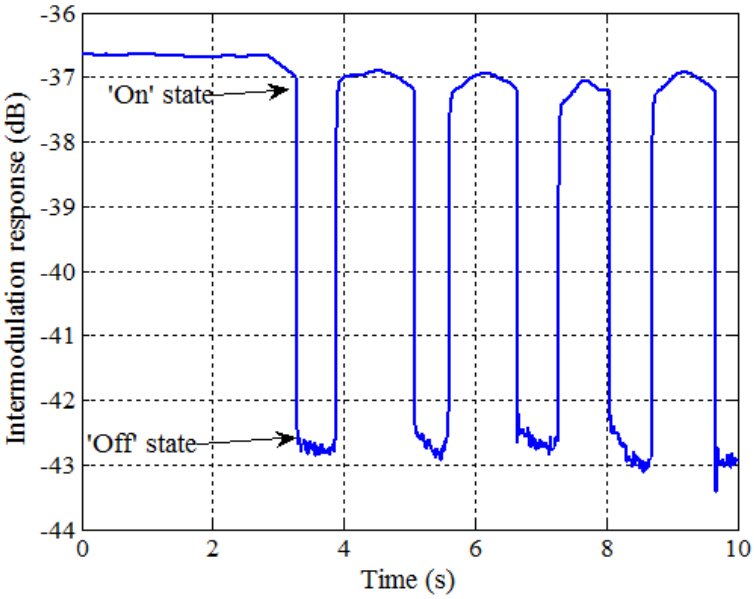

Figure 3.16. Measured intermodulation response of a sensor as a function of time when the sensor is switched between ON and OFF states [IV].

3.5.3 Inclination/Acceleration Sensor

A passive wireless MEMS-based acceleration or inclinometer sensor is devised by utilizing a capacitive MEMS accelerometer as the sensor element. Fig. 3.17 shows the simplified electrical equivalent circuit of the transponder. The $\pm$ 1 g MEMS (micro electromechanical system) accelerometer is a silicon MEMS sensor element (courtesy of Murata Electronics Oy) composed of two fixed walls and one moving part. The structure is hermetically sealed and damped with gas. Acceleration is approx-

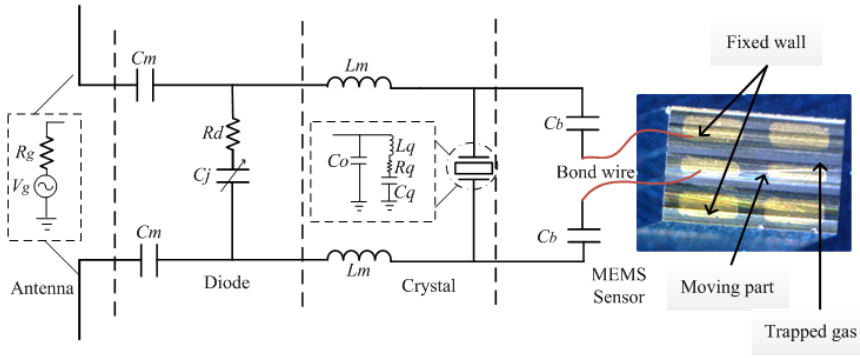

Figure 3.17. Equivalent circuit for the optimized sensor and a photograph of the MEMS acceleration/inclination structure [VI].

imately related to the capacitance C_s according to:

$$a = K(\frac{C_{s0}}{C_s} - 1), \tag{3.11}$$

where $K = \frac{k_c d}{m}$, and $k_c = \frac{3EA}{L^3}$ is the effective spring constant term, E is the Young's modulus, m is the mass of the sensor, d is the gap between one wall and the central moving part, A is the section area ,and C_{s0} is the base capacitance of the sensor.If only gravitational force affects the sensor, we can find the relationship between the angle α of the inclination and the sensor capacitance:

$$sin\alpha = [\frac{K}{g}(\frac{C_{s0}}{C_s} - 1)], \tag{3.12}$$

where g is the gravitational force.

It can be seen from (3.11) and (3.12) that once the MEMS element is selected, the capacitance value C_s is the only unknown parameter. C_s can be obtained by fitting the equivalent circuit with the measured intermodulation response.

The measurements are carried out by repeating the intermodulation measurements at different inclination angles of the sensor from $-90°$ to $90°$ at a step of $10°$. The measurements are realized at a 2-meter reading distance. Fig. 3.18 shows the intermodulation response of the transponder for three cases: $0°$, $-90°$, and $90°$. The results show clearly that the resonance frequency shifts upward when the tag is rotated clockwise.

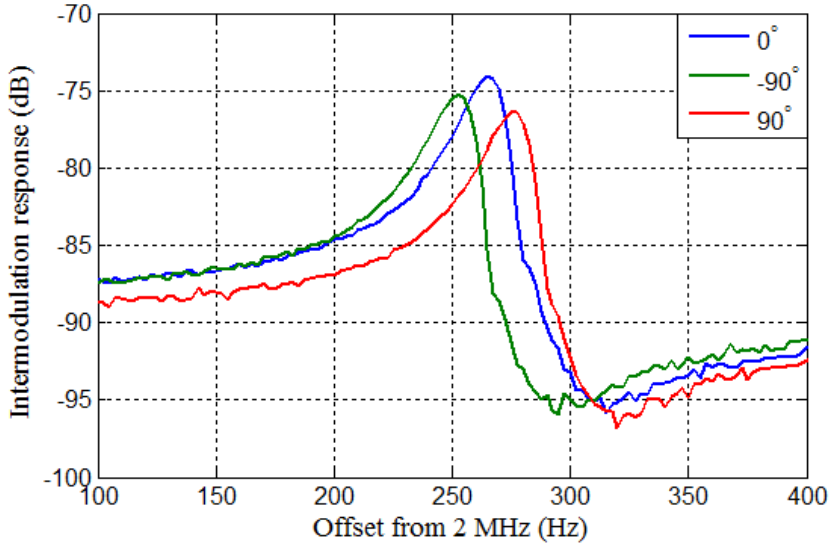

Figure 3.18. Intermodulation responses measured for three different inclinations of the sensor as a function of the offset frequency from 2 MHz at a 2 m-distance [VI].

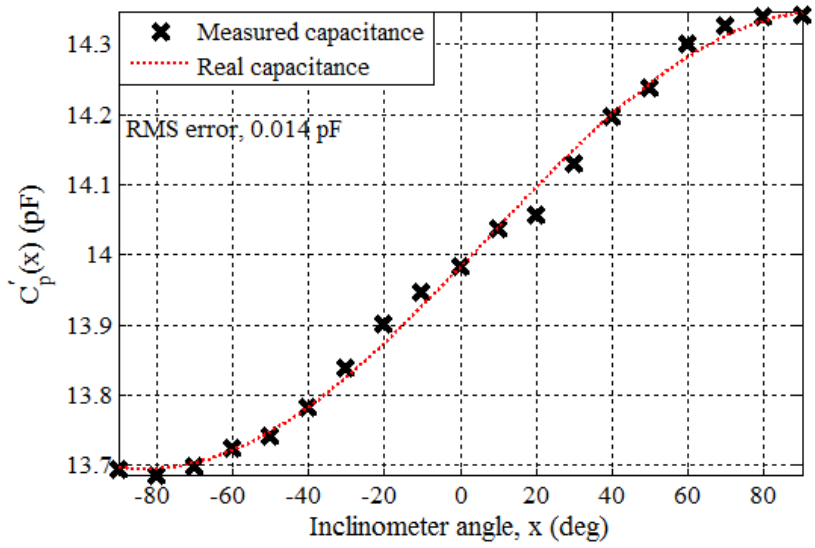

Figure 3.19. Estimates of $C_S{}'(x)$ at different distances compared to fitted sine curves [VI].

The calculated capacitance values as a function of the inclination angle are plotted in Fig. 3.19. It is obvious that the measured capacitances align very well (within the measurement setup accuracy, RMS is less than 0.014 pF) with the real capacitance values at different inclinations and the results show that at a 2-meter distance the sensor values can be read-out relatively precisely.

3.6 Integration of Intermodulation Communication Sensor

Intermodulation sensors were demonstrated to measure different quantities in the previous section. These passive sensor transponders were implemented using discrete passive components mounted on the antenna substrate. This section presents an integrated realization of the concept.

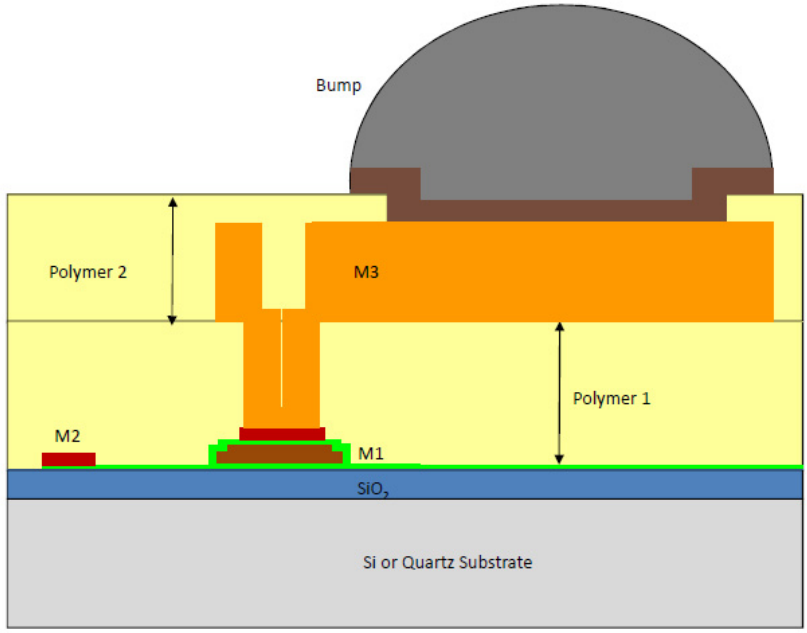

Figure 3.20. Simplified schematic of the utilized Integrated Passive Devices (IPD) process [VII].

3.6.1 Integrated Passive Device Process

The integration relies on Integrated Passive Device (IPD) processes [80] - [82]. The passive components can be integrated with active components, for example, through wafer bonding, flip-chip bonding or other similar

techniques. IPD processes typically have thick metal layers on high resistivity Silicon or Quartz to achieve good quality factors (see Fig. 3.20). Copper conductors typically provide a quality factor in the order of 100 and the used Metal-Insulator-Metal (MIM) capacitors even higher than that.

3.6.2 Integrated Intermodulation Sensor

The intermodulation sensors, loaded with a MEMS accelerometer, are partly integrated using the IPD process. The MEMS component is the same as that used in the inclination measurement. All the passive components of the circuit shown in Fig. 3.17, that is C_m, L_m, and C_b, were realized in the IPD process. The external components include the mixing diode, the quartz resonator and the capacitive MEMS sensor. A photograph of the manufactured chip is shown in Fig. 3.21.

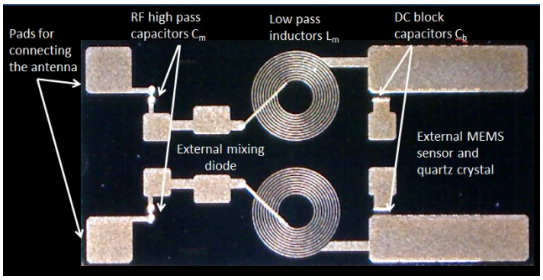

Figure 3.21. Photograph of the manufactured integrated sensor platform [VII].

Fig. 3.22 shows a photograph of the sensor platform consisting of an antenna, integrated passive components, diode, quartz crystal and a MEMS acceleration sensor. The antenna is bonded to the integrated sensor platform. The transponder is designed to operate at the UHF frequency band from 866 to 868 MHz. Fig. 3.23 shows the intermodulation response of the transponder for three different inclination angles: $-90°$, $0°$, and $90°$. The results show that the resonance frequency shifts upward when the tag is rotated clockwise.

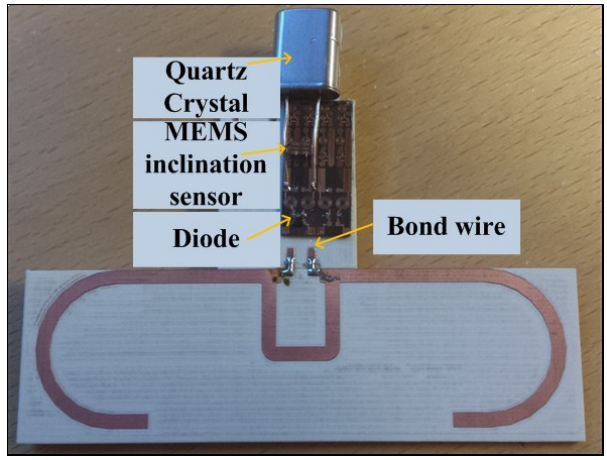

Figure 3.22. Photograph of the manufactured transponder including the antenna, IPD platform, diode, quartz, and MEMS sensor [VII].

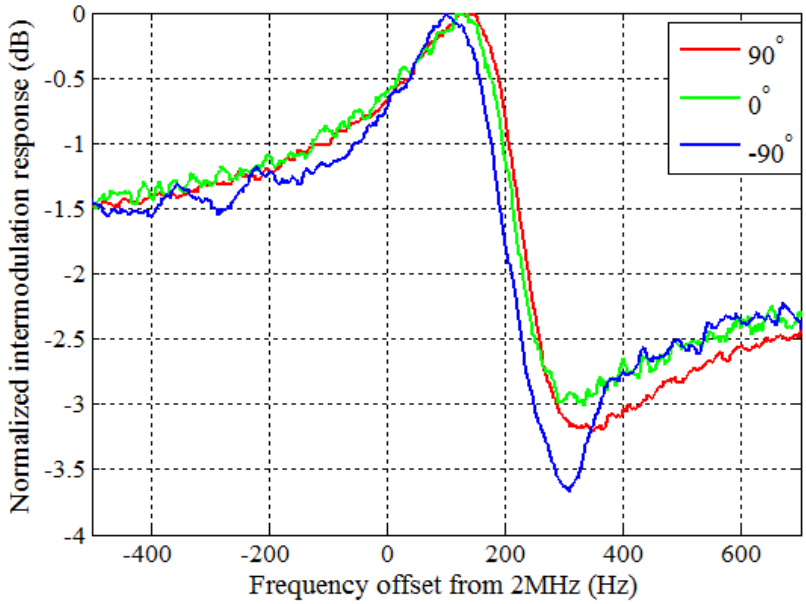

Figure 3.23. Simplified schematic of the utilized Integrated Passive Device (IPD) process [VII].

4. Estimation of Sensor State in Intermodulation Sensors

The sensor information is coded analogically to the response signal in the intermodulation communication principle. The reader records the amplitude and phase of the intermodulation signal as a function of the frequency difference between the excitation signals. The sensor value is obtained with a proper algorithm from this response.

The sensor value is related non-linearly to the measured response. The measured response, in addition to the signal from the wireless device, contains noise and possibly interference. These things make it challenging to estimate the sensor value from the measured intermodulation response. This chapter introduces a simplified signal model describing how sensor value is related to the measured response. An algorithm for solving the sensed value from the response is introduced.

4.1 Model for the Intermodulation Signal Measured by the Reader

In the intermodulation communication principle, the reader transmits two tones f_{RF} and $f_{RF+\Delta} = f_{RF} + f_{\Delta}$, where $f_{\Delta} << f_{RF}$ is assumed because f_{Δ} is in the range of several KHz to tens of MHz, while f_{RF} is in the GHz range. The intermodulation response reflected from the sensor is at an intermodulation frequency $f_{RF-\Delta} = f_{RF} - f_{\Delta}$.

Let us consider the equivalent circuit of the sensor utilizing the intermodulation communication principle in Fig. 3.6. Since f_{Δ} is considerably small compared to the carrier bandwidth f_{RF}, the intermodulation response at the sensor is simplified as [III]:

$$S_{im} = \frac{V_A(\omega_{RF-\Delta})}{V_A(\omega_{RF})} = C^2(A + B \cdot Z_N(\omega_{\Delta}, C_s)), \tag{4.1}$$

where $V_A(\omega_{RF-\Delta})$ and $V_A(\omega_{RF})$ are the received signal at the intermodulation frequency and the carrier frequency. Symbol C^2 is used to denotes

the free space pass loss (FSPL). A and B are the same complex constants as in Section 3.2.3. Z_N is the impedance of the equivalent Norton current source at the difference frequency f_Δ which depends on the sensor capacitance values C_s. For the sensor structure shown in Fig. 3.6, the impedance $Z_N(\omega_\Delta)$ can be simplified as

$$Z_N(\omega_\Delta, C_s) = (Y_q(\omega_\Delta) + j\omega_\Delta C_s' + Y_j(\omega_\Delta) + Y_m(\omega_\Delta))^{-1}, \tag{4.2}$$

where $Y_j(\omega_\Delta)$, $Y_m(\omega_\Delta)$, and $Y_q(\omega_\Delta)$ are the admittance of the diode, the low frequency block capacitor C_m, and the quartz crystal, respectively. Assuming a reciprocal channel in the reader system, the reader receives the following signal at the intermodulation frequency.

$$V_{A,RF-\Delta} = C^4(A + B \cdot Z_N(\omega_\Delta, C_s)). \tag{4.3}$$

Noise is always added to the measured response. The dominant noise source depends on the reader and is likely to be either the thermal noise of the antenna and the receiver front-end, or phase noise of the local oscillator. Finally, after taking the noise into account, the signal model of the intermodulation response can be considered as

$$V_{A,RF-\Delta} = A'(B' + Z_N(\omega_\Delta, C_s)) + v_n, \tag{4.4}$$

where A' and B' are unknown complex constants and $v_n \sim CN(0, \sigma^2)$ is complex white normal distributed noise with variance σ^2.

4.2 Estimation Methods

The above model in (4.4) relates the sensor value to the measurements. The expression shows the measured intermodulation response is related to a sensor element value, such as the capacitance of a capacitive sensor element. Hence, sensor values can be extracted from a simple fitting of the signal model to the measured response. This has been done in previous paper [77]. However, such a fitting procedure has been found to be computationally demanding, to converge easily in local minima, and not be a maximum-likelihood estimator in the presence of white noise or any other noise that can be justified from physical grounds. Hence, this section presents a maximum likelihood algorithm based on the Levenberg-Marquardt for estimating the sensor value and also the measurement un-

certainty.

4.2.1 Maximum-likelihood Estimator

In order to simplify the analysis, several assumptions have been made. A mixing diode is considered a tunable capacitor without losses ($R_D \sim 0$), and $Y_m(\omega_\Delta) \approx j\omega_\Delta C_m$. In order to estimate the unknown sensor capacitance C_s, the model in (4.4) is further simplified as

$$Z_N(\omega_\Delta, x) = (Y_q(\omega_\Delta) + j\omega_\Delta C_s')^{-1}, \tag{4.5}$$

where $C_S' = C_0 + C_S + C_j + C_m$, and $Y_q(\omega_\Delta)$ can be measured once the quartz crystal is selected . The task of the parameter estimation is then to estimate the optimal values for the parameter set

$$\boldsymbol{\theta} = [C_s' \quad \Re(A') \quad \Im(A') \quad \Re(B') \quad \Im(B')]^T \tag{4.6}$$

from a vector of measurements with N frequency points

$$\boldsymbol{y} = [y_{\omega,1} \cdots y_{\omega,N}]^T = \boldsymbol{s}(\boldsymbol{\theta}) + \boldsymbol{n}, \tag{4.7}$$

where $y_{w_i} = V_{A,RF-\Delta}(\omega_{\Delta,i})$ are the measurements defined in (4.4). Vector $\boldsymbol{s}(\boldsymbol{\theta})$ maps the parameters of the measurements, and $\boldsymbol{n}$ is a vector of zero-mean complex Gaussian noise samples, with covariance matrix $\boldsymbol{R} = \sigma^2 \cdot \boldsymbol{I}$, where $\boldsymbol{I}$ is the identity matrix. Given (4.5), we can model the measurements as a multivariate complex Gaussian variable $y \sim CN(s(\theta), R)$, and formulate a likelihood function $l(\boldsymbol{\theta} \mid \boldsymbol{y})$ for the parameters θ given in the measurements y as [83]

$$l(\boldsymbol{\theta} \mid \boldsymbol{y}) = \frac{1}{\pi^N det(\boldsymbol{R})} \cdot exp(-(\boldsymbol{y} - \boldsymbol{s}(\boldsymbol{\theta}))^H \boldsymbol{R}^{-1} (\boldsymbol{y} - \boldsymbol{s}(\boldsymbol{\theta}))). \tag{4.8}$$

The maximum likelihood estimate of the parameters (4.5) is obtained by minimizing the cost function by maximizing (4.8).

$$\hat{\boldsymbol{\theta}}_{ML} = argmin_{\boldsymbol{\theta}}\{(\boldsymbol{y} - \boldsymbol{s}(\boldsymbol{\theta}))^H \boldsymbol{R}^{-1} (\boldsymbol{y} - \boldsymbol{s}(\boldsymbol{\theta}))\}. \tag{4.9}$$

A gradient-based iterative optimization algorithm, such as the Levenberg-Marquardt (LM) algorithm [84] can be applied to obtain the solution of (4.9). The LM requires the computation of partial derivatives of the model w.r.t the parameters. The Jacobian matrix $D(\theta) \in C^(N \times P)$ for P param-

eters is firstly defined as

$$\boldsymbol{D}(\boldsymbol{\theta}) = \frac{\partial \boldsymbol{s}(\boldsymbol{\theta})}{\partial \boldsymbol{\theta}^T}. \tag{4.10}$$

It can then be shown that the partial derivatives w.r.t. log likelihood $L(\boldsymbol{\theta} \mid \boldsymbol{y}) = log_e(l(\boldsymbol{\theta} \mid \boldsymbol{y}))$ are given by [85]

$$Q(\boldsymbol{\theta} \mid \boldsymbol{y}, \boldsymbol{R}) = \frac{\partial L(\boldsymbol{\theta}) \mid \boldsymbol{y}}{\partial \boldsymbol{\theta}} = 2 \cdot \Re\{\boldsymbol{D}^H(\boldsymbol{\theta})\boldsymbol{R}^{-1}(\boldsymbol{y} - \boldsymbol{s}(\boldsymbol{\theta}))\}, \tag{4.11}$$

and the Fisher Information Matrix $\boldsymbol{J}(\boldsymbol{\theta}, \boldsymbol{R})$ as

$$\boldsymbol{J}(\boldsymbol{\theta}, \boldsymbol{R}) = 2 \cdot \Re\{\boldsymbol{D}^H(\boldsymbol{\theta})\boldsymbol{R}^{-1}\boldsymbol{D}(\boldsymbol{\theta})\}. \tag{4.12}$$

Using the definitions (4.11)-(4.12) and an initial value $\hat{\boldsymbol{\theta}}^{\{0\}}$, the LM iterations are given by

$$\hat{\boldsymbol{\theta}}^{\{i+1\}} = \hat{\boldsymbol{\theta}}^{\{i\}} + (\boldsymbol{J}(\hat{\boldsymbol{\theta}}^{\{i+1\}}, \boldsymbol{R}) + \xi^i \cdot \boldsymbol{I} \circ \boldsymbol{J}(\hat{\boldsymbol{\theta}}^{\{i+1\}}, \boldsymbol{R}))^{-1} \cdot \boldsymbol{Q}(\hat{\boldsymbol{\theta}}^{\{i\}} \mid \boldsymbol{y}, \boldsymbol{R}), \tag{4.13}$$

where ξ is an adaptive scaling factor used for controlling the convergence. The derived estimator in (4.13) is iterative due to the non-linear relation between the estimated parameters and observations. Iteration can be considered time consuming in some cases. However, in the present case the algorithm can operate at much faster speed than the reader hardware. Therefore, the algorithm does not hinder the system performance in any way.

4.2.2 Experiments And Estimation Results

The estimation algorithm is applied to the estimation of the measured response of a passive wireless inclination sensor (See Fig. 3.17 in Section 3.5.3). The wireless passive inclination sensor is placed at a fixed distance from the reader and the intermodulation response is recorded as a function of the difference frequency for different positioning angles from - 90° to + 90°, at a step of 10°. This measurement procedure is repeated for three different distances: 30 cm, 1 m, and 2 m.

Fig. 4.1 shows the amplitude of the measured responses at the three different distances, and the modelled responses using initial and estimated parameter values. Each measured frequency response at a specific inclination angle is limited between the vertical dashed lines. Comparing Fig. 4.1 (a), (b), and (c), the linear amplitudes are one and two orders of magnitude weaker at distances of 30 cm, 1 m and 2 m, respectively, and

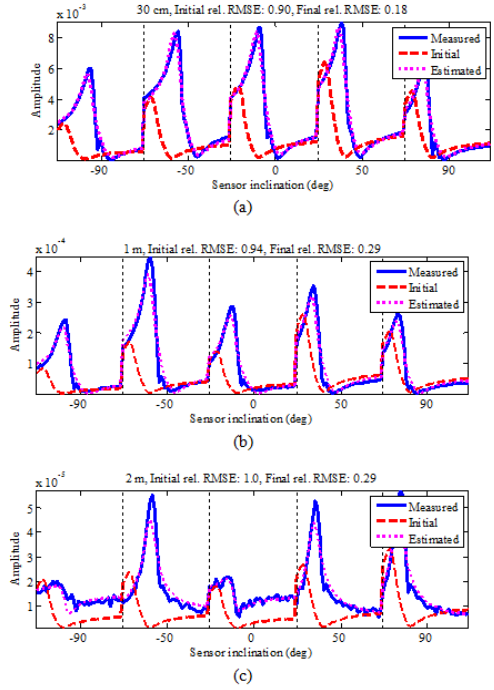

Figure 4.1. Measured (solid blue) and fitted (pink dot) intermodulation responses at different measurement distances and sensor inclinations. The dashed vertical lines mark the separation between different inclinations. The measurement distances and relative RMSE are 30 cm and 0.18 (a), 1 m and 0.29 (b), and 2 m and 0.29 (c), respectively [III].

especially weak for the measurements closer to zero angle at furthest distance. The latter is potentially due to the combination of the multipath propagation and the minima in the sensor antenna pattern in the direction of the reader antenna.

Fig. 4.2 shows estimation results for $C'_S(x)$. Alongside the estimates, dashed curves are shown which are obtained by numerically fitting a sine function (the shape that the force on the accelerometer should be a function of the inclinometer angle). From Fig. 4.2, it is obvious that there is some difference in the model at close distances as the estimates from 1 m and 2 m distance align very well (within the measurement setup accuracy), whereas the measurements at 30 cm distance show an offset of about 0.2 pF (also the angular alignment of the sensor seems to have some mismatch). The model mismatch is likely to derive partly from the intermodulation generation in the receiver.

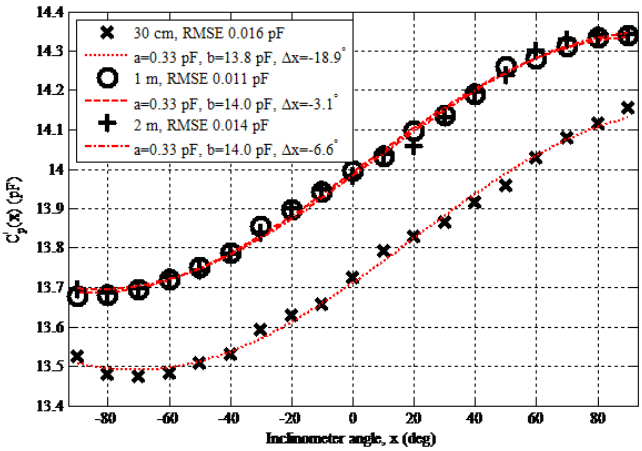

Figure 4.2. Estimates of $C'_S(x)$ at different distances compared to fitted sine curves [III].

5. Reader System

Intermodulation communication sensors require a specific reader device capable of transmitting at two frequencies and receiving at an intermodulation frequency. This section describes a prototype reader developed for the intermodulation sensors.

5.1 Read Range

The read range is a very important parameter. Here we derive the read range for an intermodulation sensor.

Let us consider a reader system with antenna gain G_r, transmitting power P_t, and sensor antenna gain G_s, the input power P_{in} received by the sensor tag is calculated according to the Friis equation [86]:

$$P_{in} = (\frac{\lambda}{4\pi r})^2 P_t G_s G_r. \tag{5.1}$$

The power converted to the intermodulation frequency P_{IM} from the input power $P_{in}$is

$$P_{IM} = LP_{in}, \tag{5.2}$$

where L is the conversion loss from input power to intermodulation power, conversion loss L is proportional to the square of the input power in the small–signal region [76].

Again, the intermodulation signal reflected to the reader is calculated using the Friis equation. The read range r is calculated by equating the intermodulation signal at the reader with the reader sensitivity. And we further assume the reader sensitivity is limited by the reader noise level

P_n. Finally, the read range r can be solved as:

$$r = \frac{\lambda}{4\pi} \sqrt[4]{\frac{LP_tG_r^2G_s^2}{P_n}}. \tag{5.3}$$

5.2 Reader Architecture

From (5.3), it is easy to recognize that once the sensor is optimized, sensor antenna gain G_s and conversion loss L are fixed values; therefore, the reader antenna gain G_r, reader output power P_t, and reader noise level P_n are the remaining parameters that affect the read range. Typically, a patch antenna is selected as the reader antenna because of its relatively high gain of 8 dB, commercial availability, and reasonable price. Noise level P_n, on the other hand, requires a huge amount of work to reduce even 10 dB. Reader output power P_t is the only parameter that can be easily enlarged to 27 dBm (allowed power in the frequency regulation for UHF RFID sensor) in the specific reader compared with 10 dBm from the VNA. The objective of this design, therefore, is to promote the highest output power while keeping the noise level as low as possible.

In order to have two output frequencies f_1 and f_2, the transmitter part of the reader needs to have two separate synthesizers, each consisting of a VCO (Voltage Controlled Oscillator)controlled by a PLL, enabling both exact, sub-Hz stable output frequencies, and pure, dual-tone output. The reader architecture is shown in Fig. 5.1. The receiver is a typical superheterodyne receiver. The signal is first mixed with $(f_1 + f_2)/2$ to the intermediate frequency (IF), and then passes through the low pass filter. The IF signal is then amplified and further down-converted to DC for sampling. The high power transmitting signal is well isolated from the receiver part by a circulator. The first reader system is implemented with evaluation boards and discrete amplifier blocks according to Fig. 5.1.

It turns out that the sensitivity of the reader is not limited by the thermal noise but limited by the intermodulation signal generated in the reader itself. Therefore, the spurious-free dynamic range of the reader is considerably smaller than the linear dynamic range. The strongest intermodulation distortion comes from the non-linearity of the PAs and the signal leakage through the circulator. The thermal noise floor for the system is estimated to be -125 dBm while the intermodulation generated by the reader itself is measured as $-$ 70 dBm from the receiver's input. The

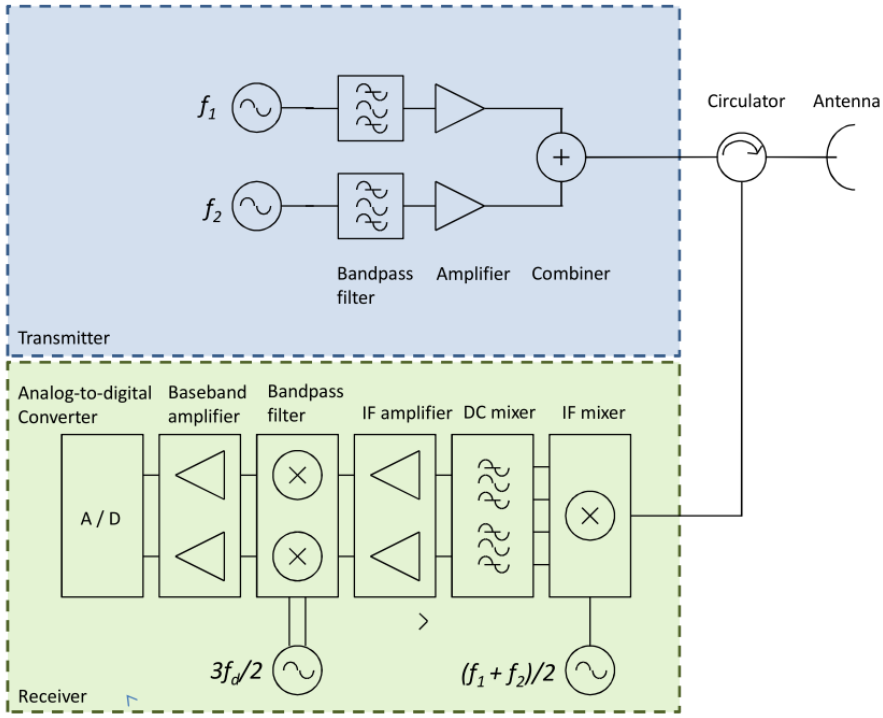

Figure 5.1. Block diagram of the reader system [IX].

intermodulation distortion is much higher than the noise floor and it limits the read range of the reader system.

Table 5.1. System parameters for the read range measurement

Trasmitted power	P_t = 16 dBm
Reader antenna gain	G_r = 8 dBi
Wavelength	λ = 0.346 m
Sensor antenna gain	G_s =2 dBi
Third order intercept point	IIP_3 = -70 dBm

A photograph of the reader and the measurement setup is shown in Fig. 5.2. The sensor is attached to a ventilation valve located several meters away from the reader. The tuning position of the valve controls the ON/OFF state of the sensor. The reader parameters are listed in Table 5.1.

The maximum read out distance is about 7 m. This happens when the intermodulation noise power is $-$ 70 dBm. Using calculations, it is predicted that 25 meters distance can be achieved if the noise level could be limited to $-$ 100 dBm. Detailed results of the measurements can be found in [IX].

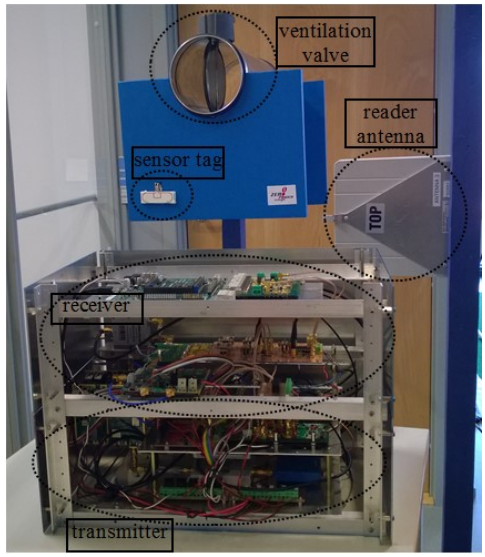

Figure 5.2. The reader-sensor tag system used in the measurements: The magnetic switch is connected to the ventilation valve [IX].

6. Summary of Articles

Publication I: “Passive wireless sensor platform utilizing a mechanical resonator”
This paper presents a new passive wireless sensor platform based on the intermodulation communication principle. The platform utilizes a quartz crystal or other mechanical resonators and enables the sensor to have a narrow bandwidth and ID-code to the sensor. Analytical modelling of the intermodulation response of the sensor is elaborated and verified by simulations and the concept is experimentally demonstrated at 1.25 GHz.

Publication II: “Optimization of wireless sensors based on intermodulation communication”
In this publication, an analytical expression for optimizing the electrical circuitry of a sensor based on the intermodulation communication principle is derived and verified by harmonic balance simulations. An optimized sensor is designed, fabricated, and experimentally characterized. Results show that a 1 % change in the sensor capacitance can still be detected at a distance of 13 m and the read-out principle can enable an extreme resolution at shorter distances (less than per mille below 5 m).

Publication III: “Maximum Likelihood Estimation for Passive Wireless Intermodulation Communication Sensors”
In this publication, equations are derived to estimate the quantity measured by the wireless sensor from its intermodulation response and the equations are experimentally verified with a passive wireless inclination sensor operating at 860 MHz. The results show that the sensor values can be estimated at a wide range of distances. The derived equations can be further used to improve the interrogation speed of the sensor by investigating less measurement points located in the vicinity of the inter-

modulation response.

Publication IV: “Realizing Frequency Division Multiple Access with Passive Wireless Intermodulation Communication Sensors”
This publication introduces an approach to generate identification (ID) codes in the intermodulation communication sensors. IDs are coded to the resonance frequency. This also enables the frequency division multiple access (FDMA) concept. The ID and multiple access scheme based on frequency division is experimentally demonstrated with 10 binary passive wireless sensors operating simultaneously at 866 MHz UHF.

Publication V: “On the Use of the Intermodulation Communication Towards Zero Power Sensor Nodes”
This publication demonstrates the use of the intermodulation communication principle for long-range reading wireless passive sensors. Analytical expressions and measurement results are reviewed and the outputs of an ECG (electrocardiography) wireless sensor are given.

Publication VI: “Long Range Passive Wireless MEMS-based Inclination or Acceleration Sensor Utilizing the Intermodulation Communication Principle”
This publication describes a MEMS-based passive wireless transponder relying on the intermodulation communication principle that is applied to inclinometer or accelerometer measurements. The transponder operates at the UHF band and provides $\pm$ 1 g acceleration and $\pm$ 90 degrees inclination within a reading distance of several meters.

Publication VII: “Integrated Passive Wireless Sensor Transponders based on the Intermodulation Communication Principle”
This paper describes a passive intermodulation communication sensor platform where passive components are realized using the Integrated Passive Device (IPD) process. The concept is experimentally verified with a MEMS accelerometer sensor used to measure the sensor’s inclination in a static gravitational field.

Publication VIII: “Review of Passive Wireless Sensors Utilizing the Intermodulation Communication”
This publication reviews different kinds of passive wireless sensors uti-

lizing the intermodulation communication principle. The reviewed sensor architectures are based either on a mechanical resonator, electrically nonlinear sensing element, or on a separate mixer, low-frequency resonance circuit and a sensing element. The benefits and drawbacks of different architectures are compared and some experimental results are presented.

Publication IX: “Achieving Long Reading Ranges with Passive Wireless Intermodulation Sensors”

This paper presents a system architecture combining batteryless wireless intermodulation sensors and their associated reader. The achievable read range of such a sensor-reader system is analyzed. The computed read range is compared to those provided by harmonic and passive UHF RFID sensor systems. Effects of both reader thermal noise and third-order distortion by the reader itself on the read range of the system are considered by means of theoretical analysis, simulations, and measurements.

7. Conclusions and future work

In this dissertation, a sensor system utilizing intermodulation communication was developed. The results of the research work are published in publications [I]– [VI]. Chapters 1-6 summarized the background and the theory behind the topics, the development of the intermodulation communication sensors and their applications, the optimization of the intermodulation communication sensor, the reader system, the signal model and the estimation method of the sensor parameters, and the scientific contribution of the work.

The intermodulation communication principle was fully explained in this dissertation, and three approaches to realize the intermodulation communication sensors were reviewed. The first approach utilizes a resonant MEMS sensor simultaneously as a mixer and sensor. The second approach is based on an element which is both electrically non-linear and sensitive to a measured quantity. The two approaches have very simple structures and can be made on a small-scale without great cost. However, the environmental loading of the antenna and the lack of commercially available sensor elements working at microwave frequencies limit their range of applications. The last approach consists of a separate mixer and low frequency resonance circuits that hence solves the problems of the first two approaches.

Applying the quartz crystal or other mechanical resonators as the low frequency resonance circuit increases the quality factor of the intermodulation sensors; thus, it offers a longer read-out distance and a narrower bandwidth. The signal model to predict the intermodulation response was elaborated and verified by simulations and the concept was demonstrated at 1.25 GHz.

For the intermodulation communication sensors with a mixer and a quartz crystal as the low frequency resonance circuit, one optimization

theory was established in [II]. Equations to optimize the circuitry of the sensor were derived and verified by harmonic simulations. The results showed a 1 % change in the sensor capacitance detectable at 13 m distance and an extremely high resolution was achieved at shorter distances.

Identification (ID) can be easily generated in the intermodulation communication sensors. IDs can be coded for example in the low frequency resonance circuit, realizing the frequency division multiple access (FDMA) concept. The FDMA concept is validated with 10 binary ON/OFF intermodulation communication sensors. In future work, reprogrammable IDs could be achieved with paraelectric varactors which are loaded onto the quartz crystals.

Sensors based on the intermodulation communication principle enable a wide range of applications. The feasibility of the intermodulation communication principle was experimentally studied for ECG, binary state machines, and an acceleration/inclination sensor. The experiments shoed that the sensor is quite sensitive to small signals (the ECG signal is only a few millivolts) and the sensor has a long read out distance. In the future, multiple sensing can be realized by using different resonant frequencies and the sensing elements can be integrated on one sensor platform.

Integrated Passive Device (IPD) processes were applied to verify the integration of the sensor based on the intermodulation communication principle. The integrated platform was demonstrated with inclination measurements. An achievable distance of 14.5 m was predicted and the possibility of realizing a highly integrated sensor in the IPD process was experimentally studied. In this study, only the passive component was integrated. In future work, the diode and low frequency resonance circuit could be further integrated to minimize the size of the sensor.

A specific reader is requested to read out the intermodulation response. The reader architecture is shown in [IX]. It was shown that the read range is limited by the intermodulation signals generated in the reader transmitter, especially by the synthesizers and PAs. A 7 m read out distance was achieved with a reader whose intermodulation noise level was -70 dBm. In future work, a reader with better intermodulation response is required, and coupling and intermodulation noise should therefore be reduced. Additionally, harmonic insertion methods are planned to be used in the transmitter.

Sensor values can be obtained by analyzing the intermodulation responses. A maximum likelihood estimator was derived for this purpose.

The estimation equations were experimentally verified by a intermodulation communication sensor equipped with a MEMS inclination sensor. The results showed that the sensor values can be estimated reliably at a wide range of distances. Moreover, the interrogation speed of the sensor was improved by utilizing the maximum likelihood estimation equations.

This dissertation shows that intermodulation sensors can be read–out precisely at long distances, comply with frequency regulations, enable IDs, and can be used in many potential applications. Hence, the intermodulation communication sensor enables the deployment of passive wireless sensing.

Currently, all intermodulation sensors are equipped with dipole type antennas whose gain is about 2 dBi. In the future, a sensor antenna with high gain will be designed such that the resolution can be further improved. Ultimately, the sensor can be integrated into MEMS (microelectromechanical systems) so that the size of the sensor will be greatly reduced.

References

[1] “Internet of Things in 2020: Roadmap for the Future,” 2008,(accessed 17 Jun., 2015) [online]. Available: http://www.smart-systems-integration.org/public/internet-of-things.

[2] I.F. Akyildiz, W. Su, Y. Sankarasubramaniam, and E. Cayirci, “Wireless sensor networks: a survey,” *Computer Networks,* vol. 38, no. 4, pp. 393–422, 2002.

[3] D. Estrin, L. Girod, G. Pottie, and M. Srivastava, “Instrumenting the world with wireless sensor networks,” in *Proceedings of IEEE International Conference on Acoustics, Speech, and Signal Processing (ICASSP)*, Salt Lake City, UT, 7–11 May 2001, vol.4, pp. 2033–2036.

[4] J. K. Hart and K. Martinez. “Environmental Sensor Networks: A revolution in the earth system science?” *Earth–Science Reviews*, vol. 78, no. 3, pp, 177–191, 2006.

[5] A. Tiwari, P. Ballal, and F. L. Lewis, “Energy-efficient wireless sensor network design and implementation for condition-based maintenance,” *ACM Transactions on Sensor Networks*, vol. 3, no, 1, pp. 1–23, Mar. 2007.

[6] M. Magno, D. Boyle, D, Brunelli, B. Flynn, E. Popovici, and L. Benini, “Extended wireless monitoring through intelligent hybrid energy supply,” *IEEE Transactions on Industrial Electronics*, vol. 61, no. 4, pp. 1871—1881, Apr. 2014.

[7] W. Chen, J.C. Hou, and L. Sha, “Dynamic clustering for acoustic target tracking in wireless sensor networks,” *IEEE Transactions on Mobile Computing,* vol. 3, no. 3, pp. 258–271, Jul.–Sept. 2004.

[8] IDTechEx report "Wireless Sensor Networks 2012–2022",(accessed 17 Jun., 2015) [Online]. Available:

http://www.prnewswire.com/news-releases/wireless-sensor-networks-wsn-2012-2022-forecasts-technologies-players-218528931.html

[9] E. Gaura and R. Newman, *Smart MEMS and Sensor Systems*, London: Imperial College Press, 2006.

[10] B. A. Warneke and K. S. J. Pister, "MEMS for distributed wireless sensor networks," in *Proceedings of 9th International Conference on Electronics, Circuits Systems*, 2002, vol. 1, pp. 291–294.

[11] Y. Manoli, "Energy harvesting–From devices to systems," in *Proceedings of European Solid-State Circuits Conference (ESSCIRC)*, Seville, Spain, 14–16 Sept. 2010, pp. 27–36.

[12] Z. Hu and B. Li, "On the fundamental capacity and lifetime limits of energy-constrained wireless sensor networks," in *Proceedings of 10th IEEE Real-Time and Embedded Technology and Applications Symposium (RTAS 2004),* Toronto, Canada, 25–28 May 2014, pp. 25–28.

[13] H. Stockman, " Communication by means of reflected power," in *Proceedings of the IRE*, 1948, vol. 36, pp. 1196–1204.

[14] K. Finkenzeller, *RFID Handbook*, 3rd ed., New York: John Wiley & Sons Inc. 2010.

[15] R. Weinstein, "RFID: A technical overview and its application to the enterprise," *IT Professional,* vol. 7, no. 3, pp. 27–33, May/Jun. 2005.

[16] A. Pohl, "A review of wireless SAW sensors," *IEEE Transcations on Ultrasonics, Ferroelectrics, and Frequency Control,* vol. 47, no. 2, pp. 317–332, Mar. 2000.

[17] J.C. Butler, A.J. Vigliotti, F.W. Verdi, and S.M. Walsh, "Wireless, passive, resonant-circuit, inductively coupled, inductive strain sensor," *Sensors and Actuators A: Physical*, vol. 102, no. 1–2, pp. 61–66, Dec. 2002.

[18] J. G. Vogler, D. J. Maquire, and A. E. Steinhauer, " DINADE–A new interrogation, navigation and detection system," *Microwave Journal*, vol. 10, no. 4, pp. 2–6, Apr. 1967.

[19] P. Sen and D. Sen, *RFID for Energy & Utility Industries*, PennWell, 2009.

[20]] V. Chawla and D. S. Ha, "An overview of passive RFID," *IEEE Communications Magazine*, vol. 45, no. 9, pp. 11–17, Sep. 2007.

[21] B. Jiang, J. R. Smith, M. Philipose, S. Roy, K. Sundara-Rajan, and A. V. Mamishev, "Energy scavenging for inductively coupled passive RFID systems," *IEEE Transactions on Instrumentation and Measurement*, vol. 56, no. 1, pp. 118–125, Feb. 2007.

[22] J. Jung, H. Kim, H. Lee, and K. Yeom, "An UHF RFID Tag with Long Read Range,"in *Proceedings of the 39th European Microwave Conference, EuMC 2009*, Rome, Italy, 29 Sept.–1 Oct., 2009, pp.1113–1116.

[23] "Omni-ID Launches New High-Performance UHF Gen 2 Tags," (accessed 16 Jun., 2015) [Online]. Available: http://www.rfidjournal.com/articles/view?5213

[24] R. Want, "Enabling ubiquitous sensing with RFID," *Computer*, vol. 37, no. 4, pp. 84–86, Apri. 2004.

[25] N. Cho, S.J. Song, S. Kim, and H.J. Yoo, "A 5.1-μW UHF RFID tag chip integrated with sensors for wireless environmental monitoring," *ESSCIRC 2005: Proceedings of the 31st European Solid–State Circuits Conference,* Grenoble, France, 12–16 Sept. 2005, pp. 279–282.

[26] L. M. Ni, D. Zhang, and M. R. Souryal, "RFID-based localization and tracking technologies," *IEEE Wireless Communications*, vol. 18, no. 2, pp. 45–51, Apr. 2011.

[27] L. Catarinucci, I. Cuinas, I. Exposito, R. Colella, J.A.G Fernandez, L. Tarricone, "RFID and WSNs for traceability of agricultural goods from Farm to Fork: Electromagnetic and deployment aspects on wine testcases," in *Proceedings of International Conference on Software Telecommunications and Computer Networks, SoftCOM 2011*, Split, Croatia, 15–17 Sept. 2011, pp. 1–4.

[28] A. Vergara, E. Llobet, J.L. Ramírez, P. Ivanov, L. Fonseca, S. Zampolli, A. Scorzoni, T. Becker, S. Marco, and J. Wöllenstein, "An RFID reader with onboard sensing capability for monitoring fruit quality," in *Eurosensors 2006*, Goteborg, Sweden, 2006.

[29] R. Angeles, "RFID technologies: Supply-chain applications and implementation issues," *Information Systems Management*, vol. 22, no. 1, pp. 51–65, 2005.

[30] A. Lehto, J. Nummela, L. Ukkonen, L. Sydanheimo, and M. Kivikoski, "Passive UHF RFID in paper industry: Challenges, benefits and the application environment," *IEEE Transcations on Automation Science and Engineering*, vol. 6, no. 1, pp. 66–79, Jan. 2012.

[31] L. Li and F. Kong, "Research on assembly quality tracing of automobile industry based on RFID," in *Proceedings of Advanced Technology of Design and Manufacture*, Beijing, China, 23–25 Nov. 2010, pp. 498–503.

[32] K. Finkenzeller, *RFID Handbook*, Munich, John Wiley & Sons Inc., 2003.

[33] A.P. Sample, D.J. Yeager, P.S. Powledge, A.V. Mamishev, and J.R. Smith, "Design of an RFID–based battery–free programmable sensing platform," *IEEE Transactions on Instrumentation and Measurement,* vol. 57, no. 11, pp. 2608–2615, Nov. 2008.

[34] Ams, analog semiconductor manufacturer, Graz, Austria, (accessed 16 Jun., 2015) [Online], Available: http://www.ams.com/eng/Products/UHF-RFID/UHF-Interface-and-SensSe-Tags

[35] Farsens, Wireless sensor manufacturer, Donostia-San Sebastián, Spain, (accessed 16 Jun., 2015) [Online]. Available: http://www.farsens.com/en/battery-free-sensor-solutions

[36] L. Yang, R. Zhang, D. Staiculescu, C. P. Wong, and M. N. Tentzeris, "A novel conformal RFID-enabled module utilizing inkjet-printed antennas and carbon nanotubes for gas-detection applications," *IEEE Antennas And Wireless Propagation Letters*, vol. 8, pp. 653−656, 2009.

[37] J. Siden, Z. Xuezhi, T. Unander, A. Kotyug, and H.-E. Nilsson, "Remote moisture sensing utilizing ordinary RFID tags," *IEEE Sensors, 2007*, Atlanta, GA, pp. 308−311, 28–31 Oct. 2007.

[38] T. Feldengut, J. Wang, S. Kolnsberg, and R. Kokozinski, "A Passive Long-Range UHF Transponder with Integrated Temperature Sensor, " *4th European Workshop on RFID Systems and Technologies (RFID SysTech)*, Freiburg, Germany, 10-11 Jun. 2008, pp. 1–4.

[39] S. Manzari and G. Marrocco, “Modeling and applications of a chemical-loaded UHF RFID sensing antenna with tuning capability,” *IEEE Transactions on Antennas and Propagation*, vol. 62, no. 1, pp. 94−101, Jan. 2014.

[40] S. Rokhsaz and E. de Angle, “Method and apparatus for detecting RF field strength,” U.S. Patent 2011/0291810 A1, Dec. 1, 2011.

[41] S. Rokhsaz, “Method and apparatus for varying an impedance,” U.S. Patent 2008/0116990 A1, May. 22, 2008.

[42] Smartrac’s new passive sensor dogbone transmits moisture levels, (accessed 25 Aug., 2015) [Online]. Available: http://www.rfidjournal.com/articles/view?12723/

[43] M.P. da Cunha, R.J. Lad, P. Davulis, A. Canabal, T. Moonlight, S. Moulzolf, D.J. Frankel, T. Pollard, D. McCann, E. Dudzik, A. Abedi, D. Hummels, and G. Bernhardt, “Wireless acoustic wave sensors and systems for harsh environment applications,” in *Proceedings of IEEE Wireless Sensors and Sensor Networks (WiSNet)*, Phoenix, AZ, 16–19 Jan. 2011, pp. 41–44.

[44] V. P. Plessky and L. M. Reindl, “Review on SAW RFID Tags,” *IEEE Transactions on Ultrasonics, Ferroelectrics, and Frequency Control*, vol. 57, no. 7, pp. 654–668, Mar. 2010.

[45] G. Scholl, F. Schmidt, T. Ostertag, L. Reindl, H. Scherr, and U. Wolff, “Wireless passive SAW sensor systems for industrial and domestic applications,” in *Proceedings of IEEE International Frequency Control Symposium*, Pasadena, CA, 27–29 May 1998, pp. 595–601.

[46] K. Lee, W. Wang, T. Kim, and S. Yang, “A novel 440 MHz wireless SAW microsensor integrated with pressure–temperature sensors and ID tag,” *Journal of Micromechanics and Microengeering*, vol. 17, no. 3, pp. 515–523, Feb 2007.

[47] A. Pohl and L. Reindl, “Measurement of physical parameters of car tires using passive SAW sensors,” in *Proceedings of Advanced Microsystems for Automotive Applications Conference*, 1998, pp. 250—262.

[48] B. Dixon, V. Kalinin, J. Beckley, and R. Lohr, “A second generation in-car tire pressure monitoring system based on wireless passive SAW

sensors," in *Proceedings of 2006 IEEE Frequency Control Symposium and Exposition*, Miami, FL, June 2006, pp. 374–380.

[49] U. Wolff, F. Schmidt, G. Scholl, and V. Magori, "Radio accessible SAW sensors for non-contact measurement of torque and temperature," in *Proceedings of IEEE Ultrasonics Symposium*, San Antonio, 3–6 Nov 1996, pp. 359—362.

[50] G. Frye, R. Kottenstette, E. Heller, J. Brinker, S. Casalnuovo, A. Sellinger, N. Raman, and Y. Lu, "Optimizing surface acoustic wave sensors for trace chemical detection," in *Proceedings of IEEE Transducers '97,* Chicago, IL, 16–19 Jun. 1997, vol. 2, pp. 1323–1326.

[51] R. Nopper, R. Niekrawietz, and L. Reindl, "Wireless readout of passive LC sensors," *IEEE Transactions on Instrumentation and Measurement*, vol. 59, no. 9, pp. 2450–2457, Sep. 2010.

[52] V. Viikari, J. Song, and H. Seppä, "Passive wireless sensor platform utilizing a mechanical resonator," *IEEE Sensors Journal*, vol. 13, no. 4, pp. 1180–1186, Apr. 2013.

[53] S. Bhadra, G.E. Bridges, D.J. Thomson, and M.S. Freund, "A wireless passive sensor for pH monitoring employing temperature compensation," in *Proceedings of IEEE Sensors*, Limerick, Ireland, 28–31 Oct. 2011, pp. 1522–1525.

[54] J. Voutilainen, *Methods and Instrumentation for Measuring Moisture in Building Structure*, Doctoral Thesis, Helsinki University and Technology, Espoo, Finland, 2005.

[55] D.E.N. Davies and R.J. Klensch, "Two-frequency secondary radar incorporating passive transponders," *Electronics Letters.*, vol. 9, no. 25, pp. 592–593, Dec. 1973.

[56] H. G. Gomes and N. B. Borges Carvalho, "RFID for location proposes based on the intermodulation distortion," *Sensors & Transducers* , vol. 106, no. 7, pp. 85—96, 2009.

[57] V. Viikari, J. Chisum, and H. Seppä, "Wireless passive photo detector for insect tracking," *Microwave and Optical Technology Letters*, vol. 52, no. 10, pp. 2312–2315, Oct. 2010.

[58] J. Shefer and R. J. Klensch, "Harmonic radar helps autos avoid collisions," *IEEE Spectrum*, vol. 19, no. 5, pp. 38–45, May 1973.

[59] H. Staras and J. Shefer, “Harmonic radar detecting and ranging system for automotive vehicles,” U.S. Patent 3 781 879, Jun. 30, 1972.

[60] Glcharvat, (accessed 16 Jun., 2015) [Online]. Available: http://www.glcharvat.com/Dr._ Gregory_ L._ Charvat_ Projects/Harmonic_ Radar.html

[61] J. R. Riley and A. D. Smith, “Design considerations for an harmonic radar to investigate the flight of insects at low altitude,” *Computers and Electronics in Agriculture*, vol. 35, no. 2-–3, pp. 151—169, Aug. 2002.

[62] E. T. Cant, A. D. Smith, D. R. Reynold, and J. L. Osborne, “Tracing butterfly flight paths across the landscape with harmonic radar,”in *Proceedings of Royal Society B*, Apr. 2005, vol. 272, no. 1800, pp. 785–790.

[63] D. Psychoudakis, W. Moulder, C.C. Chen, H. Zhu, and J. L. Volakis, “A portable low-power harmonic radar system and conformal tag for insect tracking,” *IEEE Antennas and Wireless Propagation Letters,* vol. 7, pp. 444–447, 2008.

[64] B. G. Colpitts, and G. Boiteau, “Harmonic radar transceiver design: miniature tags for insect tracking,” *IEEE Transactions on Antennas Propagation*, vol. 52, pp. 2825–2832, 2004.

[65] R. D. Brazee, E. S. Miller, M. E. Reding, M. G. Klein, B. Nudd, and H. Zhu, “A transponder for harmonic radar tracking of the black vine weevil in behavioral research,” *Transactions on American Society of Agricultural Engineers*, vol. 48, no. 2, pp. 831-–838, 2005.

[66] D. Mascanzoni and H. Wallin, “The harmonic radar: A new method of tracing insects in the field,” *Ecological Entomology*, vol. 11, no. 4, pp. 387—390, Nov. 1986.

[67] Z. M. Tsai, P. H. Jau, N. C. Kuo, J. C. Kao, K. Y. Lin, F. R. Chang, E. C. Yang, and H. Wang, “A high-range-accuracy and high-sensitivity harmonic radar using pulse pseudorandom code for bee searching,” *Transactions on Microwave Theory and Techniques*, vol. 61, no. 1, pp. 666–675, Jan. 2013.

[68] RECCO Rescue System, A System for Locating Avalanche Victims. Liding Sweden, Recco AB, (accessed 16 Jun., 2015) [Online]. Available: http://www.recco.com/about

[69] M. Bouthinon, J. Gavan, and F. Zadworny, “Passive microwave transposer, frequency doubler for detecting the avalanche victims,” in *Proceedings of European Microwave Conference,* Warszawa, Poland, 8–12 Sept. 1980, pp. 579–583.

[70] I. Nassar and T. Weller, “Design and characterization of a passive harmonic sensor embedded in sand,” in *Proceedings of IEEE Wireless and Microwave Technology Conference (WAMICON)*, Orlando, FL, 7–9 Apr. 2013, pp. 1—3.

[71] H. Kwun, G. L. Burkhardt, and J. L. Fisher, “Detection of reinforcing steel corrosion in concrete structures using non-linear harmonic and intermodulation wave generation,” U.S. Patent 5 180 969, Jan. 19, 1993.

[72] F. Yu, Y. Ma, and E.C. Kan, “A passive wireless sensor with reflective nonlinear transmission lines for capacitive signal transduction,”in *Proceedings of IEEE Radio and Wireless Symposium (RWS)*, Santa Clara, CA, 15–18 Jan. 2012, pp. 103–106.

[73] B. Kubina, J. Romeu, C. Mandel, M. Schüßler and R. Jakoby, “Quasi–chipless wireless temperature sensor based on harmonic radar,” *Electronics Letters*, vol. 50, no. 2, pp. 86–88, Jan. 2014.

[74] H. C. Gomes and N. B. Carvalho, “The use of intermodulation distortion for the design of passive RFID,” in *Proceedings of 4th European Radar Conference*, Munich, Germany, 10–12 Oct. 2007, pp. 377–380.

[75] V. Viikari and H. Seppä, “RFID MEMS sensor concept based on intermodulation distortion,” *IEEE Sensors Journal*, vol. 9, no.12, pp. 1918–1923, Dec. 2009.

[76] V. Viikari, H. Seppä, T. Mattila, and A. Alastalo, “Wireless ferroelectric resonating sensor,” *IEEE Transactions on Ultrasonics, Ferroelectrics, and Frequency Control*, vol. 57, no. 4, pp. 785–791, Apr. 2010.

[77] V. Viikari, H. Seppä, and D. Kim, “,” *IEEE Transactions on Microwave Theory and Techniques*, vol. 59, no. 4, pp. 1025–1031, Apr. 2011.

[78] J. Rahola, “Power waves and conjugate matching,” *IEEE Transactions on Circuits and Systems-II: Express Briefs*, vol. 55, no. 1, pp. 92–96, Jan. 2008.

[79] K.V.S. Rao, P.V. Nikitin, and S.F. Lam, "Antenna design for UHF RFID Tags: A review and a practical application," *IEEE Transactions on Antennas and Propagation*, vol. 53, no. 12, pp. 3870–3876, 2005.

[80] S. Liu, C. Wang, C. Lee, and W. Wang, "Miniaturized WiFi system module using SiP/IPD for handheld device applications," in *Proceedings of Microsystems, Packaging, Assembly and Circuits Technology iMPACT 2007*, Taipei, 1–3 Oct. 2007, pp. 146–148.

[81] K. Liu, R. Frye, M. Hlaing, Y. Lee, H Kim, G. Kim, and B. Ahn, "Investigation of integrated passive device with through-silicon via," in *Proceedings of IEEE 62nd Electronic Components and Technology Conference (ECTC)*, San Diego, CA, 29 May–1 Jun. 2012, pp. 1833–1839.

[82] A. C. Kundu, M. Megahed and D. Schmidt, "Comparison and analysis of integrated passive device technologies for wireless radio frequency module," in *Proceedings of Electronic Components and Technology Conference*, Lake Buena Vista, FL, 27–30 May 2008, pp. 683–687.

[83] L. L. Scharf, *Statistical Signal Processing: Detection, estimation, and time series analysis,* Addison-Wesley, New York, 1991.

[84] D. Marquardt, "An algorithm for least squares estimation of nonlinear parameters," *Journal of Society for Industrial and Applied Mathematics (SIAM)*, vol. 11, no. 2, pp. 431–441, June 1963.

[85] A. Richter, Estimation of radio channel parameters: Models and algorithms, Ph.D. dissertation, Technischen Universitat Ilmenau, Germany, 2005.

[86] J. D. Kraus and R. J. Marhefka, *Antennas for All Applications, 3rd ed*, McGraw-Hill, 2002.

Errata

Publication II

In the second paragraph of subsection II. B, p. 3447, it should read "...and $L = (C_m + C_j)/\omega_{RF}^2 C_m C_j$."

The dissertation focuses on the development of passive wireless sensors based on the intermodulation communication principle. The research in this dissertation contributes in three parts: Firstly, the dissertation discusses on the sensor based on the intermodulation communication principle and its applications. The study shows that the sensor can be used as a generic multi-sensing platform with some potential applications such as monitoring ECG, the state of a switch, inclination, and acceleration. Secondly, the dissertation discusses the read-out and estimation of the sensor states. A signal model which deals with the intermodulation response is established and the maximum-likelihood estimation method is applied to precisely read out the sensor state. Thirdly, the dissertation describes the reader part of the system. Considerations affecting the read range of the sensor are discussed. A reader architecture is described and the limitations affecting the reader performance have been studied.

Aalto-DD 122/2015

ISBN 978-952-60-6354-6 (printed)
ISBN 978-952-60-6355-3 (pdf)
ISSN-L 1799-4934
ISSN 1799-4934 (printed)
ISSN 1799-4942 (pdf)

Aalto University
School of Electrical Engineering
Department of Radio Science and Engineering
www.aalto.fi